Reactivation of the Pleistocene trans-Arabian Wadi ad Dawasir fluvial system (Saudi Arabia) during the Holocene humid phase

Albert Matter [a], Ayman Mahjoub [b], Eike Neubert [c], Frank Preusser [d,e *], Antje Schwalb [f], Sönke Szidat [g], Gerwin Wulf [e]

[a] Institute of Geological Sciences, University of Bern, Balterzerstrasse 1+3, 3012 Bern, Switzerland

[b] Saudi Geological Survey, P.O.Box 54141, Jeddah 21514, Kingdom of Saudi Arabia

[c] Natural History Museum Bern, Bernastrasse 15, 3005 Bern, Switzerland

[d] Previously at: Department of Physical Geography and Quaternary Geology, Stockholm University, 10690 Stockholm, Sweden

[e] Institute of Earth and Environmental Sciences, University of Freiburg, Albertstraße 23b, 79104 Freiburg, Germany

[f] Institut für Geosysteme und Bioindikation, Technische Universität Braunschweig, 38106 Braunschweig, Germany

[g] Department of Chemistry and Biochemistry & Oeschger Centre for Climate Change Research, University of Bern, Freiestrasse 3, 3012 Bern, Switzerland

*corresponding author. E-mail: frank.preusser@geologie.uni-freiburg.de

Accepted version

Published in

Geomorphology 270 (2016) 88–101

http://dx.doi.org/10.1016/j.geomorph.2016.07.013

Abstract – The Wadi ad Dawasir fluvial system in central Saudi Arabia is investigated using remote sensing and sedimentology, in combination with bio-proxy analyses (molluscs and ostracods). Age control is provided by radiocarbon as well as luminescence dating, using both quartz and feldspar grains. It is shown that the fluvial system was active from the Asir Mountains across the partially sand-covered interior of the Arabian Peninsula to the Arabian Gulf during the Holocene humid period. Sedimentology and faunal analysis reveal the presence of perennial streams and a permanent freshwater lake in the distal reach of the Dawasir system that are synchronous with fluvial accumulation in the headwaters of its major tributary, Wadi Tathlith. The increased runoff during the Holocene led to a re-activation of streams that largely followed pre-existing Late Pleistocene courses and eroded into older sediments. The absence of Holocene lakes in most of the Rub' al-Khali implies that trans-Arabian rivers were mainly fed by precipitation in the Asir Mountains. Monsoonal rainfall was apparently stronger there as well as in the northern, south-eastern and southern part of the Arabian Peninsula (southern Yemen and Oman), but it apparently did not directly affect the interior during the Holocene. The palaeoenvironmental reconstruction shows a narrow trans-Arabian green freshwater corridor as the result of phases of sustained flow lasting up to several centuries. The permanent availability of water and subsistence for wildlife provided a favourable environment for human occupation as documented by Neolithic stone tools that are found all along Wadi ad Dawasir.

Keywords: Fluvial, Holocene, Arabia, Humid period

1. Introduction

Four major sand seas (Ar Rub' al-Khali, Ad Dahna, Al Jafura, and An Nafud) cover an area of 765,000 km^2 on the Arabian Peninsula (Wilson, 1973), by this comprising 36 % of the territory of the Kingdom of Saudi Arabia. They are the most prominent evidence of the present arid to hyper-arid climate, with rainfall of less than 100 mm a^{-1} in the interior of the peninsula. Higher rainfall levels are restricted to the Hedjaz-Asir Plateau and the Yemeni highlands (Almazroui et al., 2012). This pattern is tied to the Hadley cell circulation and its local manifestation, the monsoon system, which are key components responsible for the climate of Arabia (Webster, 2005). At present, the source of rainfall reaching SW Arabia and the coast of Dhofar is the African summer monsoon rather than the Indian Ocean Summer Monsoon as previously assumed (Fleitmann et al., 2007; Bosmans et al., 2014; Enzel et al., 2015; Jennings et al., 2015). The winter months are characterized by a stable high pressure system, clear skies and mild temperatures. During this time of the year Mediterranean cyclones track across the Arabian Peninsula and reach as far as Oman, giving rise to low levels of rainfall.

Little palaeoclimate research was carried out in Saudi Arabia until recently, although the joint mapping project of the Kingdom of Saudi Arabia and the U.S. Geological Survey revealed compelling geomorphologic evidence of much wetter episodes during the Quaternary (Brown et al., 1989). A fluvial-style drainage network with large gravel accumulations east of the Hejaz-Asir Mountains (Holm, 1960) and lake deposits within the dunes of the Rub' al-Khali and the Nafud were investigated subsequently in detail by McClure (1976, 1984) and Schulz and Whitney (1986), respectively. The observation of gravel plains and aquatic molluscs in the lower reaches of Wadi ad Dawasir had already led Philby (1933) to conclude that this river system and possibly others had reached the Arabian Gulf. Brown (1960) argued that gravel terraces 20 to 60 m above the present thalweg of Wadi Sahba and Wadi Batin represent remnants of approximately 1 km wide Pleistocene river courses. Despite their low gradient of about 1 m km^{-1}, these rivers transported coarse clasts indicating a high stream power. For example, Holm (1961, cited in Edgell, 2006) reported quartzite boulders measuring up to 25 cm in size in a palaeochannel of Wadi Sahba ca. 95 km from the coast, i.e. about 600 km downstream of the source terrain in the Arabian Shield. Furthermore, these palaeorivers built-up conglomerate megafans before entering the Arabian Gulf (Hötzl et al., 1978a; Edgell, 2006). Based on K-Ar ages of two basalt flows encasing a gravel layer in the Wadi ad Dawasir, Anton (1984) argued that the major trans-Arabian wadis depicted in his palaeohydrological map were incised between 3 and 1 million years ago.

However, systematic knowledge about these obvious palaeoenvironmental changes resulted from studies carried out mainly in the adjacent countries (Oman, United Arab Emirates, Yemen) on stalagmites (Burns et al., 2001; Fleitmann et al., 2003a,b, 2004, 2005, 2007, 2011; Neff et al., 2001), lake sediments (Parker et al., 2004, 2006; Lézine et al., 1998; Radies et al., 2005; Petit-Maire et al., 2010; Rosenberg et al., 2011a; Catlett, 2014), aeolian dunes (e.g. Juyal et al., 1998; Goudie et al., 2000; Preusser et al., 2002; Radies et al., 2004) and fluvial deposits (Blechschmidt et al., 2009; Berger et al., 2012; Hoffmann et al., 2015; Parton et al., 2015). Advances in geochronology, especially Optically Stimulated Luminescence (OSL) and Uranium-Thorium ($^{234}U/^{230}Th$) methods, now permit dating these archives beyond the dating limit of radiocarbon and, hence, reconstruction of the temporal and spatial framework of the environmental history. The climate record derived from the previously mentioned archives reveals significant hydrological changes with pronounced humid periods in southern Arabia during Marine Isotope Stages (MIS) 1, 5a, 5e, 7 and 9, and further though less well-documented humid phases during MIS 3 and 11. It is assumed that high summer insolation during these periods strengthened the monsoon and pulled the associated rainfall belt northward into the interior of Arabia. ^{18}O data from stalagmites suggest that the highest precipitation levels occurred during MIS 5e and the lowest during MIS 1 (Fleitmann et al., 2011).

In the past decade, the number of studies on the palaeoenvironment of Saudi Arabia has increased markedly due to a more open political situation allowing access to remote areas such as the Rub’ al-Khali. Many of these studies have been carried out in the context of investigating the human dispersal Out-of-Africa models because knowledge of the palaeohydrology and the timing of humid phases is essential for understanding the migration of anatomically modern humans (AMH) into Arabia and beyond (e.g. Petraglia et al., 2011). This range expansion was only possible when the Arabian deserts, which represented a barrier for AMH, turned into a 'Green Arabia' with sufficient surface water and nutrition available during pluvial phases. Research has focused mainly on palaeolakes in the Rub' al-Khali (Rosenberg et al., 2011b; Crassard et al., 2013; Matter et al., 2015, Groucutt et al., 2015), the Nafud (Petraglia et al., 2012, Rosenberg et al., 2013; Hilbert et al., 2014; Scerri et al., 2015; Stimpson et al., 2015) and Tayma (Ginau et al., 2012; Engel et al., 2012), whereas only two modern studies have dated stalagmites and fluvial deposits, respectively. The stalagmites of central and northern Saudi Arabia turned out to be 400 ka old or older, indicating that rainfall was too low or sporadic to allow growth of stalagmites in the past 400 ka (Fleitmann et al., 2004). The first luminescence-dated fluvial sediments in the headwaters of Wadi as Sahba were interpreted to reflect humid events at ca. 54 ka, ca. 39 ka (corresponding to MIS 3), and ca. 0.8 ka (McLaren et al., 2009).

Breeze et al. (2015) demonstrated the potential of combined remote sensing and geographic information system (GIS) techniques to map palaeodrainage networks and palaeolakes across vast areas in much greater detail and with improved accuracy compared to earlier palaeodrainage maps of Anton (1984) and Edgell (1990, 2006). Furthermore, climate model simulations provide useful information when validated against field data to better understand the functioning of climate change. The results of a set of simulations carried out by Jennings et al. (2015) confirm that the Arabian Peninsula was wettest during MIS 5e and that lesser amounts of precipitation occurred during MIS 5c and MIS 3. Moreover, they support the results of earlier simulation experiments by Herold and Lohmann (2009) that the African monsoon rather than the Indian Summer Monsoon was the source of higher rainfall. This is in accord with the spatial and temporal distribution of lakebeds in southern Arabia. The fact that Pleistocene but no Holocene palaeolakes occur in the interior of the Rub' al-Khali suggests that the monsoonal rainfall belt migrated farther onto the Peninsula in the Pleistocene than during the Holocene (e.g. Rosenberg et al., 2011b; Matter et al., 2015). Enzel et al. (2015) challenge this interpretation based on a re-analysis of published Holocene lacustrine records. They argue that: a) the palaeolakes represent marsh environments requiring a much lesser annual rainfall to be sustained than open lakes, and b) the intensification of rainfall is not related to a northward shift of the Intertropical Convergence Zone (ITCZ) and the Indian Summer Monsoon but to a slight landward expansion of the African Monsoon across the Red Sea with uplift of the moist air over the Yemeni – Asir highlands associated with modest rains feeding the downstream wetlands. If this was the case, then the drainage systems must have experienced a major reactivation.

In this study, we investigate this hypothesis using a multi-proxy approach to reconstruct the evolution of the palaeodrainage of Wadi ad Dawasir, one of the major trans-Arabian wadis. As palaeodrainage systems respond sensitively to climate changes that affect precipitation, runoff and fluvial style, we first determine the catchment area and reconstruct the drainage pattern by remote sensing techniques. In order to get a more complete view of the area, the adjacent Wadi as Sahba system is included in the analysis. We then investigate selected sedimentary sections in the proximal and distal reaches of the Wadi ad Dawasir system and determine their facies, fossil content (molluscs and ostracods), and age (radiocarbon and luminescence dating). The ultimate goal is to establish a relationship between geomorphology, facies and runoff within a robust geochronological framework. With the above, we aim to better understand the environmental conditions in the central part of the Arabian Peninsula, for which very little information is available at the moment. The newly gathered information will be crucial for cross-checking atmospheric circulation models as well as for better characterization of past environments as important in the context of early human habitation and dispersal through the region.

2. Methods

2.1. Remote sensing and field methods

A GIS environment was implemented to analyse the Wadi ad Dawasir and Wadi as Sahba palaeodrainage systems and related catchment areas. ArcGIS 10 was applied for geospatial analyses of digital elevation models (DEMs) and to analyse multispectral data for further mapping. Digital elevation data from the Shuttle Radar Topography Mission (SRTM; Farr and Kobrick, 2000; Rabus et al., 2003; Farr et al., 2007) with a resolution of 3 arc-second (~90 m at the equator) are provided by the Global Land Cover Facility (GLCF) for download. SRTM 2.1 data were used as base data to create a DEM mosaic of the Arabian Peninsula with a cell size of 90 x 90 m (Fig. 1A). During processing, SRTM data voids were filled with elevation data from the Advanced Spaceborne Thermal Emission and Reflection Radiometer (ASTER) Global

Digital Elevation Model Version 2 (GDEM V2) (Abrams et al., 2010, 2015; Tachikawa et al., 2011). To avoid possible discontinuous drainage networks in the following processing steps, all sinks within the resulting DEM were removed to get a DEM without depressions. Flow direction and flow accumulation were then derived using the eight-direction (D8) flow model by Jenson and Domingue (1988). A drainage network was delineated by applying a threshold value to the flow accumulation raster that defines a minimum required contributing upstream area of a cell as a stream. With regard to the large area of interest (Fig.1B), a contributing catchment area of 150 km² was found appropriate to show only major stream systems while maintaining clarity. SRTM-derived drainage in large sand seas, such as the Rub' al-Khali, often shows particularly dense channel networks in interdune depressions although no fluvial landforms are visible (e.g. Petraglia et al., 2012; Crassard et al., 2013; Stimpson et al., 2015; Breeze et al., 2015). Considering the potential for errors, such peculiar dune field drainage patterns were removed from the drainage network. The western part of the area of interest is characterized by the depression of Sahl Rakbah, an internal drainage basin that is considered to be an area of rift-related subsidence (Camp and Roobol, 1989, 1991). Such large sink areas deliver erroneous, straight-running stream lines within the derived drainage network and thus were also removed. The resulting modified drainage system will be termed the 'calculated drainage' in the following. In addition, watersheds and catchment areas of the complete Wadi ad Dawasir and Wadi as Sahba systems were determined by combining the derived flow direction with defined outlet points of the watersheds (pour points) (Fig. 1B).

In areas with only minor or incomplete sand coverage, palaeodrainage systems can be traced using multispectral image data (Fig. 2A-C). Landsat 7 Enhanced Thematic Mapper Plus (ETM+) data with a spatial resolution of 30 m (e.g. Goward et al., 2001) were used to determine and map recent and palaeostream systems in addition to the calculated drainage. True and false colour composites (FCC) were generated. In the process, composites were created in such a way that the different Landsat bands were assigned to the intensities of red, green and blue (RGB) components of a colour image. A band combination of 7, 4, 2 (7 = Red, 4 = Green, 2 = Blue) were found to be most suitable to detect palaeochannels within the mapping area (Fig. 2B, C).

Digital elevation data and derived hillshade images were additionally used to retrace drainage systems that could not be unequivocally determined by Landsat images, for example if underlying palaeochannels led to a region of inverted topography (Fig. 2D). As a result, unambiguously identified stream systems were classified as ‘mapped’, whereas incomplete or patchy channels with still recognizable flow directions were classified as ‘inferred’ (Fig. 1B, 2C). It has to be considered that the mapped palaeodrainage system was inferred in a qualitative fashion and thus does not allow any quantitative conclusions concerning contributing catchment areas or relative age determinations.

Sedimentary characteristics were determined on six measured sections in the distal part of Wadi ad Dawasir and two outcrops in the proximal part of Wadi Tathlith, which is one of the major tributaries (Fig. 1B, 3). The sections in the distal reach were logged using standard sediment techniques in hand-dug pits, in a trench bulldozed across a palaeochannel at site 4213.3, and at an outcrop site 4214.3 shown in Fig. 1B. Grain size was estimated with a visual comparator. The collected macrofossil specimens are housed in the malacological voucher collection of the Natural History Museum in Bern, Switzerland. Ostracods were extracted by washing sediment samples through a sieve with a mesh width of 0.2 mm. The residue was dried and the specimens picked under a binocular microscope.

2.2. Radiocarbon dating

Radiocarbon dating was performed on shells of *Melanoides tuberculata* and *Unio tigridis* from four samples as well as one sample of *Bulinus* sp. with the accelerator mass spectrometer (AMS) MICADAS at the Laboratory for the Analysis of Radiocarbon with AMS (LARA) at the University of Bern (Szidat et al., 2014). Potential contaminants on the surface of the shells, including organic impurities and recrystallized carbonates, were removed by sequential treatment with 30% hydrogen peroxide and 0.12 mol/L hydrochloric acid at room temperature. Afterwards, the samples were acidified with concentrated phosphoric acid and transformed into AMS target material using automated graphitization equipment connected to a carbonate handling system (Wacker et al., 2013). A ^{14}C-free material (IAEA-C1) and a standard with a certified ^{14}C value (IAEA-C2) were measured together with the unknown samples for normalization. Measurement results were corrected for background from the chemical treatment using shells from a sediment sample with an age ~100 ka according to luminescence dating. Calendar ages were deduced from uncalibrated ^{14}C ages using the IntCal13 calibration curve (Reimer et al., 2013) and the results are shown on Table 1. The ages derived from the two species are within the statistical error for all samples except sample 4213.3.

XRD measurements were performed on a Panalytical XPertPRO MPD with Cu radiation at 40 mA / 40 kV using aliquots of the fine ground material prepared for ^{14}C analysis mounted on silica plates. The purpose of these analyses is to verify if the aragonitic shells had undergone recrystallization that would have altered their real age. All samples consist of >99% aragonite, except the shell of *Melanoides tuberculata* of sample 4213.3 that included 2.3% calcite. This sample is considered as an outlier in the discussion of the results.

2.3. Luminescence dating

Samples for dating by OSL, Infrared Stimulated Luminescence (IRSL) and post-IR IRSL (pIR) were taken from sandy beds by forcing a steel tube into a cleaned exposure surface. The material from the steel tubes was transferred into opaque plastic bags and sent to the laboratory at Stockholm University. Sample preparation followed standard procedures including removal of carbonates using HCl, sieving (retrieving 200-250 µm) and density separation of a K-feldspar ($\delta < 2.58$ g cm^{-3}) and quartz ($\delta < 2.70$ g cm^{-3}, $\delta > 2.58$ g cm^{-3}) fraction, the latter being subsequently etched by 40% HF (60 min), followed by HCl treatment (> 120 min) to dissolve fluorites. The final separates were fixed on stainless steel discs using silicon spray covering an area of a diameter of ca. 1 mm. This represents a few dozen grains on each aliquot. As the amount of grains with suitable grain size was relatively low, only 12 feldspar and 24 quartz aliquots have been prepared per sample.

Measurements were conducted using a Freiberg Instruments *Lexsyg Research* luminescence reader (Richter et al., 2013). Stimulation was provided by LEDs with an emission peak at 458 nm for quartz (60 mW cm^{-2}) and a laser diode at 850 nm for feldspar (150 mW cm^{-2}). For quartz, detection was at 380 nm with the combination of a Hoya U-340 (2.5 mm) and a Delta DP 365/50 interference filter (5 mm). Detection for feldspar was centred at 410 nm using a Schott BG-39 (3 mm) together with an AHF BrightLine HC 414/46 interference filter (3.5 mm). Determination of Equivalent Dose (D_e) followed the Single Aliquot Regenerative Dose (SAR) protocol of Murray and Wintle (2000) for quartz, with a preheat at 230°C for 10 s and stimulation at 125°C for 60 s. The first 0.4 s of the OSL signal were integrated with the integral 50-60 s subtracted as background. For feldspar, the pIR protocol of Reimann and Tsukamoto (2012) was used, with a preheat at 180°C for 30 s followed by an initial IR stimulation for 100 s at 50°C (IRSL) and a subsequent stimulation for 200 s at 150°C (pIR). Here, the integral 0-20 s was used for D_e determination after subtracting the last 20 s as background.

The usual rejection criteria have been applied (Wintle and Murray, 2006), and most samples show good luminescence properties. While most quartz emissions are dominated by the fast component (Fig. 4A), the samples from site 4216 show low OSL intensity and the presence of a medium component (Fig. 4B). The latter are hence considered not suitable for dating. The feldspar exhibits bright signals for both IRSL (Fig. 4C) and pIR (Fig. 4D). For samples 4214.1/1 and 4214.2/1, the OSL signal is at saturation, therefore only minimum ages have been determined (Fig. 4E), the feldspar growth curves of the same samples, however, do not show any indication of saturation (Fig. 4F). For all samples, D_e distributions have been investigated (Fig. 5A, B) and based on the observed spread of data, in particular the overdispersion value, either the Central Age Model (CAM) or the Minimum Age Model (MAM) as described by Galbraith et al. (1999) have been applied to account for the effect of differential bleaching of the luminescence signal prior to deposition (Table 2).

The concentration of dose rate relevant elements (K, U, Th) was measured by high-resolution gamma spectrometry at the University of Bern (cf. Preusser and Kasper, 2001). We did not observe any clear indication for radioactive disequilibrium in any of the samples using the approach described by Zander et al. (2007) (Table 2). Age calculations were performed with ADELE-v2015 (v.021a beta) using the dose conversion factors of Guérin et al. (2011), assuming an a-value of 0.07 ± 0.02 for feldspar and average sediment moisture content between 0-4 %. Cosmic dose rate was calculated using present day depth after Prescott and Hutton (1994). For feldspar, an internal K-content of 12.5 ± 0.5 % has been used (Huntley and Baril, 1997).

Considering that IRSL ages might be affected by signal instability (fading), these are reported here only for completeness. While the pIR signal is expected to show less fading, the use of relatively low stimulation temperatures, as done in this study to minimize problems with regard to partial bleaching, may still show some instability. However, we abstained from carrying out storage tests as the suitability of such experiments to carry-out fading corrections is highly controversial (e.g., Wallinga et al., 2007; Lowick et al., 2012; Preusser et al., 2014). Hence, in the discussion of the age of sediment deposition we will only rely on OSL and pIR ages that are consistent for all of our samples.

3. Results

3.1. *Geomorphological setting and drainage systems*

The present-day geological and geomorphological setting is of fundamental importance to the understanding of the climate and the evolution of the drainage of Saudi Arabia which is geologically divided in four distinct terrains. The Arabian Shield with its crystalline rocks crops out in the western part of the Kingdom over a large area (ca. 770’000 km^2) including the orographically highest terrain of the country. It is overlain by the homoclinal Phanerozoic sedimentary cover rocks, which dip slightly eastwards away from the shield and form a 400 km wide belt. This region is bordered by the flat lying sediments of the Interior Platform and the Neogene Rub’ al-Khali basin (Vincent, 2008). The distribution of these units is mirrored by the topography, as shown in Fig. 1A.

The geographic configuration led to the establishment of a two-part drainage network separated by a water divide following the edge of the Red Sea escarpment. The first part comprises the short and steep wadi systems that drain onto the Tihama coastal plain. The second and major part consists of confluent wadis such as Wadi ad Dawasir that flow down-dip on the beds of the sedimentary cover and across the interior to the Arabian Gulf.

The Wadi ad Dawasir and Wadi as Sahba drain large catchments of 354,050 km^2 and 130,145 km^2, respectively, with complex distributary patterns (Fig. 1B). The Wadi ad Dawasir system comprises several major tributaries including Wadi at Tathlith that drain the crystalline terrain of the Asir Mountains. Wadi ad Dawasir breaches the Jurassic carbonates of the Tuwayq Mountains at As Sulayyil to flow in a north-easterly direction across the southern end of the Dahna desert and the Rub'al-Khali. At the pour point, it is joined from the northwest by the downstream trunk of Wadi Maqran and Wadi al Jadwal that drain the sedimentary cover. In this part of the catchment the As Sahba fan acts as barrier forcing the channels of the Dawasir system to flow eastwards (Fig. 1B, 3).

The drainage system displays a trellis pattern in the upper catchment indicative of steep slopes, and channel gradients range from 1.7 to 3.8 m km^{-1}. This changes downstream to a parallel pattern on the plain, with the gradient of the trunk channel less than 0.7 m km^{-1} (Fig. 1). The width of the wadi narrows downstream from almost 30 km wide to the west of As Sulayyil to about 1.5 km a few kilometres downstream of this village. Further downstream the braided channel tapers out and is covered by dunes of the Dahna desert (Fig. 2A). With remote sensing techniques, however, the channel can be followed across the Dahna and Rub' al-Khali. In addition to this calculated channel, other river courses can be inferred from the flow direction in areas with intermittent dune coverage. The pattern of these inferred channels indicates large-scale movement of the river course across the fluvial plain due to avulsion. Downstream of the pour point, the main channel runs east of a ridge of Tertiary rocks along the western margin of Sabkha Matti (Fig. 1B). It is incised into older gravel deposits that can be followed along its course to the coastline (Bramkamp et al., 1961). Runoff in the Wadi ad Dawasir basin is restricted to the tributaries in the Asir where the majority of discharge occurs after storm events. However, the mean annual runoff is low with 0.95 m^3 sec^{-1} in Wadi at Tathlith (Vincent, 2008). Episodic floods may reach As Sulayyil, but the water dissipates within days to weeks due to very high transmission loss into the alluvium and high evaporation rate.

The Wadi as Sahba catchment is drained by the larger Wadi Birk system, which comprises several tributaries in the crystalline basement terrain and the smaller Wadi Hanifah system that has its headwaters in the Tuwayq Mountains. They cross the Tuwayq escarpment to continue downstream of their confluence as Wadi as Sahba. Channel incision in Wadi Birk and Wadi Hanifah has exposed up to 6 m of the terrace gravels. McLaren et al. (2009) dated fluvial deposits in the upper Sahba catchment to ca. 54 ka and 39 ka. A silt bed in the terrace sequence in Wadi Hanifah yielded a freshwater gastropod fauna with a radiocarbon age of 8400 ± 140 ^{14}C yr BP (Hötzl et al., 1978b), corresponding to 9650-9020 cal. yr BP. However, the most conspicuous geomorphic feature of Wadi as Sahba is its large gravel fan, which is of Late Pliocene to Early Pleistocene age according to Hötzl et al. (1978a). Its distributaries entered the Gulf to the east and west of the Qatar Peninsula (Fig. 3). The apex of the fan is located at the end of the incised channel at the edge of the Tertiary plateau from where the confined flows expanded (Bramkamp and Ramirez, 1959). The DEM of the fan shown in Fig. 3 reveals the older distributary channels in inverted relief due to deflation of the finer inter-channel deposits, and it also shows several channels that cross the coastal plain to the coast. The large areal extent of the fan and the coarse clast size of the conglomerates reveal a high erosion rate, high runoff and transport capacity during the Pleistocene pluvial events. The present-day channel runs across the fan towards Al Humr lake which, however, is fed by an artesian spring in the Tertiary rocks on its eastern shore.

3.2. Field observations, fauna, facies analysis, and dating results

The study sites are located in the lower reaches of the Wadi ad Dawasir system and in its far back hinterland in Wadi at Tathlith (Fig. 1B). The measured and dated sections from the unconfined floodplain of Wadi ad Dawasir (Fig. 6) are all situated in interdunal areas where deflation has exposed a dense braided channel network with main and auxiliary channels. These channels, which drained the floodplain visualized by satellite imagery have a low sinuosity and a width up to 50 m (Fig. 7A). As they lack topographic expression, however, they can be identified in the field only by thin veneers of pebbles mixed with coarse sand and aquatic fossils (Fig. 6). The sub-angular to sub-rounded clasts are mostly of igneous and metamorphic origin with abundant quartzite and vein quartz of maximum sizes ranging from less than 1 cm up to 10 cm (Fig. 7B). The outcrop at site 4213.2 appears as a narrow light grey band stretching a few tens of meters across the barren, tan sand-covered plain (Fig. 7C). It is littered with *Melanoides tuberculata* and *Unio tigridis* as well as *Corbicula fluminalis* and *Radix natalensis*. Many of the specimens of *U. tigridis* are preserved with both valves, resting in-situ embedded in the calcareous sand (Fig. 7B). This indicates that the shells were not transported by the river but remained in the original position after death.

In sections 4213.1 and 4213.3 the gravel lag rests on unfossiliferous quartz sand, whereas in sections 4213.2, 4214.1 and 4214.2 it overlies fossiliferous calcareous sand, clayey sand or marl (Fig. 6). The basal unit consists of structureless or faintly laminated bimodal coarse quartz sand. The grains are very well rounded and most of them show a frosted surface. Cailleux (1952) described this grain type as RM (French 'Ronds-Mats' = round and dull), and he attributed this appearance to cavities covering the surface. According to SEM imaging by Krinsley and Doornkamp (1973), these dish-like concavities are formed by grain collisions during strong winds. The presence of grains with this morphology, however, does not necessarily imply that the sands in the studied sections represent aeolian deposits. Sequence 4213.3, recorded in a trench excavated with a bulldozer across a fluvial channel, bottomed in hard unfossiliferous marl, probably of Neogene age. The channel is filled with well-rounded quartz sand that had been reworked by Wadi ad Dawasir along its course across the Dahna and Rub' al-Khali deserts. In contrast, the basal sand unit of none of the other sections mentioned above was bottomed. These sands lack facies with diagnostic sedimentary structures other than faint lamination. According to OSL/pIR dating, the sands in sections 4213 are of Holocene age (dated between 7900 ± 600 a and 3700 ± 300 a by luminescence, with discrepancies compared to radiocarbon dated discussed below), whereas 4214.1 and 4214.2 date to the early Late Pleistocene (pIR ages of 90 ± 6 ka and 109 ± 11 ka, OSL ages being minimum estimates due to signal saturation). We speculate that sands of Holocene age are fluvial and those of Pleistocene age are aeolian deposits (Fig. 6). This interpretation is supported by the channel geometry at site 4213.3, the lighter colour of the Holocene sands and a palaeosol with a sharp erosional surface that separates the Pleistocene basal sand from the overlying Holocene fluvio-lacustrine marl in section 4214.2 indicating a period of non-sedimentation. This site is located on the floodplain and the section was measured in a hand-dug pit.

The beds of section 4214.3 occur as a low mesa remnant with a relief of about 2 m located about 200 m eastwards of site 4214.2. The sequence is of Holocene age according to OSL/pIRL (6100 ± 300/5600 ± 300 a) and radiocarbon (8400-8700 cal. yr BP) dating. It consists of alternating 5 to 10 cm-thick beds of fossiliferous calcareous sands and marl with a 40 cm-thick marl at the top (Figs 6, 7D). These beds contain a rich freshwater malacofauna with *Unio tigridis*, *Corbicula fluminalis*, *Melanoides tuberculata*, *Radix natalensis* and *Bulinus* sp., and rests on loose sand of Holocene age. This consists of very well rounded quartz grains with the frosted surface texture characteristic of aeolian abrasion.

The freshwater malacofauna of the lower Dawasir basin is congruent with the findings of Hötzl et al. (1978b), with the only exception that these authors did not find any freshwater bivalves, while in our assemblage the pulmonate *Biomphalaria pfeifferi* is missing.

The ostracod fauna found in four out of six sections of the lower Wadi ad Dawasir basin (Fig. 6) consists of eight species, four of which were identified to genus level. Abundance varies from very low (four valves in 4213.2/2) to high (161 valves in 4214.3/2), whereas other samples yield moderate abundances (33-45 valves). The most prominent species in four out of five samples is *Cyprideis torosa* which mainly occurs in marine brackish waters down to a water depth of 30 m, but also occurs in freshwater (McClure and Swain, 1980; Meisch, 2000). The second most abundant species is *Pseudocandona marchica*, which inhabits permanent and temporary water bodies, and the littoral zone of lakes, to a depth of 30 m (McClure and Swain, 1980; Meisch, 2000). The following species are present in low abundance: *Hemicypris* sp., *Ilyocypris* sp., *Cypretta* sp., *Cyprinotus*, *Cypridopsis vidua* and *Cypris pubera*. These species thrive in a broad variety of aquatic environments from small and shallow permanent ponds to creeks. The presence of *Cypris pubera* indicates a salinity of <4‰ (Meisch, 2000).

Wadi at Tathlith carved its valley in the crystalline rocks of the Arabian shield. The up to 200 m-wide floodplain is occupied by coarse grained gravel platforms and sand bars that are moved as bedload during ephemeral floods. Older deposits, possibly of Pleistocene age (Whitney, 1983), are exposed where the river has incised into the lowest gravel terrace which is ca. 6 m above the wadi's floodplain. Two outcrop sections were measured on the eastern bank of the wadi (Fig. 8). Section 4216.2 consists of weakly cemented sandy polymict gravels showing poor sorting, stratification and layers with imbricated angular to sub-rounded clasts up to 10 cm in size (Fig. 8; Whitney 1983 Fig. 14). The pIR age of 29.8 ± 1.6 ka dates the section to late MIS 3. About 2.5 km downstream, section 4216.1 was logged in the same terrace but in sandy facies with rare gravel pockets. The sequence consists of three units separated by dark palaeosols with iron stained grains (Figs. 7E, 8). These must record hiatuses in sedimentation, as palaeosol development requires landscape stability with neither deposition nor erosion. The sample that was taken at the base of the middle unit revealed an pIR age of 7100 ± 700 a. Due to ponding behind a constriction of the wadi about 17 km upstream of site 4216.2, extensive fine-grained alluvium was deposited (Fig. 7F). It is characterized by tan laminated silts, cross-bedded fine-grained sands and occasional gravel interbeds. Radiocarbon dating of charcoal from the top of the sequence reported originally by Whitney (1983) gave ages of 6120 ± 110 ^{14}C yr BP (7260-6740 cal. yr BP) and 5700 ± 250 ^{14}C yr BP (7160-5990 cal. yr BP). The fine-grained alluvium contrasts sharply with the older coarse-grained sediments indicating a decrease of flow intensity at the end of the Holocene pluvial. This change towards increased aridity is further supported by the occurrence of abundant displacive lenticular as well as swallow-tailed twinned gypsum crystals in the uppermost silts indicating an evaporitic environment.

4. Discussion

4.1. Timing of fluvial activity

Considering the age of fluvial deposition, there is an obvious discrepancy between radiocarbon (of shell material) and luminescence ages (Fig. 6, 9). For the four sites where both methods have been applied, the radiocarbon ages are systematically older, though these have been measured for shells collected above the horizons dated by luminescence. All radiocarbon ages are between 7 and 9 ka, but the luminescence ages are mainly several thousand years younger (up to 4 ka). Age underestimation of luminescence ages could be caused by signal instability but the OSL signal of the samples is clearly dominated by the fast component that is stable over millions of years (e.g., Preusser et al., 2009). Furthermore, the OSL ages agree very well with the pIR ages that have different physical properties. There is also no indication for radioactive disequilibrium in the samples that could have led to miscalculation of dose rate.

On the other hand, radiocarbon samples could have been re-worked, but this appears unlikely as the material is well preserved and embedded. Rather, shell material could be affected by the hardwater effect, i.e. an up-take of dissolved ancient carbonates. In this case the ^{14}C level is lower than the atmosphere and the basic assumption of radiocarbon dating that a sample incorporates carbon in equilibrium with the atmosphere is no longer fulfilled. A hardwater effect between 0 and almost 6000 years is possible in freshwater systems (Clark and Fritz, 1997; Philippsen, 2013). This effect is well known from several studies in Arabia, with the radiocarbon ages from shell carbonate being a few hundred to 1500 years older than the age of associated organic material (Davies, 2006; Rosenberg et al., 2011b; Dinies et al., 2015). However, the pIR/OSL ages for site 4213.3 are almost 4.0 ka older than its radiocarbon age of about 7300 cal. yr BP (*Unio tigridis*). To achieve the almost double as old radiocarbon age, carbon taken up by the mussel should be composed of ~1/3 fossil and ~2/3 contemporary material, which appears quite high. Nevertheless, the samples under consideration here are from the context of a river system that crosses through areas with abundant limestone that will be dissolved in the water. Hence, the hardwater effect should indeed be much higher than in samples from Mundafan, where non-carbonate bearing basement and volcanic rocks are outcropping. Interestingly, we found almost identical ages for *U. tigridis* and *M. tuberculata* at several sites, which is unexpected as their habitats and their diets are different and this should be reflected by differences in the hardwater effect.

In summary, there is no unequivocal explanation for the observed offset between pIR and OSL ages on the one hand, and radiocarbon ages on the other hand. Despite this, a certain offset caused by hardwater uptake must be expected from the environmental setting (creatures living in and feeding from resources associated to carbonate-rich water). Hence, we are relying on the luminescence ages in the later chronological interpretation.

4.2. Palaeoenvironmental inferences

The narrow width of the channels in the lower reach of the Wadi ad Dawasir system in combination with a gravel lag consisting of well-rounded pebble-sized clasts indicate a rather sluggish regime of the Holocene rivers. This is supported by the preservation of *U. tigridis* with both valves intact. However, no conclusive inference is possible with regards to channel depth as sequence thickness has been reduced by strong aeolian deflation in this area. Inverted fluvial channels (Fig. 2D) are further evidence of this process. The section at site 4214.3 composed of alternating 5 to 10 cm-thick fossiliferous sand and marl beds with planar contacts is interpreted as flood deposits and low-energy homogeneous fines, respectively deposited in a shallow lake.

The fauna comprising gastropods, bivalves, ostracodes and rare charophytes is identical in both the fluvial and lacustrine deposits. The composition of the fossil freshwater malacofauna is typical for the area and similar to present day populations (Neubert, 1998; Neubert et al., 2015). All species recorded are extant besides the large freshwater mussel *U. tigridis*. Until now, this species has not been recorded from the Arabian Peninsula; however, our results demonstrate that its extinction was a quite recent event. Remarkably, this species is not recorded from the nearby oasis Al Hasa, even though this oasis has an enormous permanent freshwater supply. This might be due to the fact that this oasis belongs to a separate drainage system receiving its water from groundwater wells, and it thus was not connected to the Dawasir or the Sahba system.

Today, *U. tigridis* lives in the lentic, i.e. relatively still water, shore area of large to medium-sized rivers and larger lakes in the Euphrates-Tigris basin in Turkey, Syria, Iraq and probably Iran (Al-Bassam and Hassan, 2006; Lopes-Lima and Seddon, 2014). These bivalves need freshwater fish species as intermediate hosts for their larvae, and thus require a stable, perennial habitat with relatively large water bodies (Matter et al., 2015). In the investigated area, these mussels have been the most abundant fossils representing a large and well-established population. From resettlement experiments in Europe we know that *Unio* species are extremely sensitive concerning the quality of their habitats. It may take 10-20 years of insertion of infected fish specimens until a first population is established. After that, hatchlings need between 4-10 years until reaching maturity. This demonstrates that habitats need to be stable for 30 years at least to support a single generation of mussels. We frequently observed mussels of differing sizes in our fossiliferous layers, which we interpret as several subsequent generations of mussels, and thus as evidence of stable habitat conditions in the order of magnitude of one to several centuries. A short-termed fluctuation in habitat conditions such as in an ephemeral flow regime with subsequent re-settlement of a rich mussel fauna is very unlikely. The remaining species can be considered more euryoecious, i.e. they are able to survive in short-lived habitat and re-colonise it after desiccation given there are surviving populations in the surroundings. Only *M. tuberculata*, which has a parthenogenetic mode of reproduction, is able to colonise even small (and also brackish) water bodies from a single specimen. For this reason it can be found as a tramp-species in all tropical and subtropical biomes. The palaeoecological information of the ostracod fauna is less conclusive because all of the species are typical of a variety of permanent and temporary aquatic habitats and most of them tolerate moderate to high salinities. The occurrence of *Cyprideis torosa*, however, indicates warm, shallow and permanent water bodies as its eggs cannot withstand desiccation (Anadón et el., 1986; Pint et al., 2012). It develops characteristic nodes in low-salinity waters with Ca^{2+} deficiency (Frenzel et al., 2012). The Dawasir samples yielded smooth shells, which may only suggest saline conditions rather than freshwater as indicated by *U. tigridis*. However, according to Frenzel et al. (2012), the use of nodes as a proxy for palaeowater chemistry requires further study of the relationships of water chemistry and shell morphology; they find that both ionic composition and salinity may influence morphological response (Pint et al., 2012). Therefore, the morphology of *C. torosa* should be used with caution as a palaeosalinity indicator of athalassic waters (Pint et al., 2012).

The geomorphologic, sedimentological and biological observations suggest that the lower reach of the Dawasir system in Holocene times was a fluvial plain with several river channels and floodplain lakes. The alternation of sand and marl beds in the lacustrine sequence indicates flooding of the lake from overtopping river channels as a result of fluctuating discharge. The re-interpretation by Enzel et al. (2015) of Holocene palaeolakes in Arabia as marshes neglects the biological evidence that unionid mussels and *Cyprideis torosa* need permanent water and are unable to survive in a marsh environment.

The presence of flowing rivers and permanent lakes in Wadi ad Dawasir during the Holocene wet period raises the question as to the source of the rainfall. Many studies carried out during the past decade associated the observed environmental fluctuations with a shift in the latitudinal position of the ITCZ and associated monsoonal rainfall belt, but there is surprisingly little information on its position across the Peninsula at different times. Increased precipitation during the Early to Middle Holocene appears to be restricted to North Arabia, the south-eastern, southern and western margins of the Peninsula from the Emirates to the Yemeni Highlands, and the Asir Mountains. Central Arabia and the Rub' al-Khali seem to have remained arid, lacking widespread Holocene lake deposits. Thus, the perennial Dawasir river represents a trans-Arabian lifeline across a hostile desert environment during the Holocene. This is further supported by the occurrence of Neolithic stone tools along the wadi course indicating that is was a favourable habitat for humans (Crassard et al., 2013). This palaeohydrological situation implies that the main source area of water feeding Wadi ad Dawasir in the Holocene must have been the Asir Mountains that received high amounts of rainfall due to the eastern movement of the African Summer Monsoon. Increased precipitation in this area is documented by the accumulation of river sediments, for example, in Wadi Tathlith dated to 7.1 ka and 6.1-5.7 ka and a Holocene lake at Mundafan fed by river channels draining these mountains (Rosenberg et al., 2011b). Radiocarbon dating of phytoclasts (plant particles) revealed that Lake Mundafan existed from 9600 to 7900 cal. yr BP, whereas the activity of Wadi ad Dawasir is documented in this work from ca. 7.9 to 4.0 ka according to luminescence dating. Fluvial accumulation at 5.9-5.3 ka, 4.8-4.5 ka and 4.0-2.7 ka in southern Yemen reveals that the rainfall regime in this area did not end with the so-called 'classic' Holocene wet period though the last lake dated to 7.3 ka (Lézine et al., 2010; Berger et al., 2012). This decrease in precipitation is in accord with the Qunf cave stalagmite record, which shows a concomitant decrease of $\delta^{18}O$ after 7 ka to modern values at 2.6 ka (Fleitmann et al., 2007).

5. Conclusions

Remote sensing methods allowed fluvial channels of the Sahba and Dawasir systems to be mapped from the Asir mountainous watershed across the partially sand covered interior of the Arabian Peninsula to the Arabian Gulf, facilitating the analysis of the palaeoenvironmental archives deposited during the Holocene wet phase. Sedimentological and faunal analyses reveal the presence of a stable habitat with perennial rivers and a permanent freshwater lake in the distal reach of the Dawasir system lasting up to several hundred years, which are synchronous with fluvial accumulations in the headwaters of its major tributary Wadi Tathlith. As there are no indications of Holocene lakes in most of the Rub' al-Khali it appears that the Dawasir, Sahba and possibly other trans-Arabian rivers were fed by precipitation in the Asir Mountains as a result of an intensified African summer monsoon. Hence, the general climatic setting was different from today, likely with higher summer rainfall in the Asir Mountains compared to the present, possibly accentuated by topographic effects. However, rainfall was likely not ubiquitous across the peninsula. The direct influence of the monsoonal rainfall belt was apparently limited to the south-eastern, southern and western margin as well as the northern part of the Arabian Peninsula, but did not reach into its interior. Increased runoff during the Holocene wet phase led to a re-activation of the Dawasir river, largely following its Late Pleistocene course and eroding into its previously deposited gravels and the sands of the Rub' al-Khali. The palaeoenvironmental reconstruction suggests a narrow, trans-Arabian green freshwater corridor as a result of presumably seasonal flooding similar to that of the River Nile. The permanent availability of water and subsistence for wildlife provided a favourable environment for human occupation as documented by Neolithic stone tools found along the length of Wadi ad Dawasir.

Acknowledgements

We thank Dr. Zohair A. Nawab, President of the Saudi Geological Survey (SGS), Dr. Abdullah M. Al-Attas, Assistant President for Technical Affairs and Saleh Al-Ghamdi, Director of Desert Studies of SGS for their interest and support. We thank Siddiq Habibullah and Abdulaziz Al-Solami for assistance in the field, and Dr. Urs

Eggenberger for the XRD analysis of the shell material, and Cornelia Fischer for assistance in ostracod analysis. Prof. Dominik Fleitmann kindly provided the isotope data used in Fig. 9. Dr. Laine Clark-Balzan is thanked for her comments on a previous version of the manuscript. Prof. Martin Williams, two anonymous reviewers and the editor Andrew Plater are thanked for their useful and constructive comments.

References

Abrams, M., Bailey, B., Tsu, H., Hato, M., 2010. The ASTER global DEM. Photogrammetric Engineering and Remote Sensing 76, 344-348.

Abrams, M., Tsu, H., Hulley, G., Iwao, K., Pieri, D., Cudahy, T., Kargel, J., 2015. The Advanced Spaceborne Thermal Emission and Reflection Radiometer (ASTER) after fifteen years: Review of global products. International Journal of Applied Earth Observation and Geoinformation 38, 292–301.

Al-Bassam, K.S., Hassan, K.M., 2006. Distribution and ecology of recent molluscs in the Euphrates river – Iraq. Iraqi Bulletin of Geology and Mining 2, 57-66.

Almazroui, M., Islam, M.N., Athar, H., Jones, P.D., Rahman, M.A., 2012. Recent climate change in the Arabian Peninsula: annual rainfall and temperature analysis of Saudi Arabia for 1978-2009. International Journal of Climatology 32, 953-966.

Anadón, P., De Dekker, P., Julià, R., 1986. The Pleistocene lake deposits of the NE Baza Basin (Spain): salinity variations and ostracod succession. Hydrobiologia 143, 199-208.

Anton, D., 1984. Aspects of geomorphological evolution; Paleosols and dunes in Saudi Arabia. In: Jado, A.R., Zötl, J.G. (eds.): Quaternary Period in Saudi Arabia 2, 275-296.

Berger, J.-F., Bravard, J.-P., Purdue, L., Benoist, A., Mouton, M., Braemer, F., 2012. Rivers of the Hadramawt watershed (Yemen) during the Holocene: Clues of late functioning. Quaternary International 266, 142-161.

Blechschmidt, I., Matter, A., Preusser, F., Rieke-Zapp, D., 2009. Monsoon triggered formation of Quaternary alluvial megafans in the interior of Oman. Geomorphology 110, 128-137.

Bramkamp, R.A., Ramirez, L.F., 1959. Geology of the Northwestern Rub' al-Khali Quadrangle. Kingdom of Saudi Arabia, USGS, Misc. Geol. Investigations Map I-213A, 1 : 500,000. Washington.

Bramkamp, R.A., Ramirez, L.F., 1961. Geologic Map of the Central Persian Gulf Quadrangle. Kingdom of Saudi Arabia, USGS, Misc. Geol. Investigations Map I-214A, 1 : 500,000. Washington.

Bosmans, J.H.C., Drijfhout, S.S., Tuenter, E., Hilgen, F.J., Lourens, L.J., 2014. Response of the North African summer monsoon to precession and obliquity forcings in the EC-Earth GCM. Climate Dynamics 44, 279-297.

Breeze, P., Drake N.A., Groucutt, H.S., Parton, A., Jennings, R.P., White, T.S., Clark-Balzan, L., Shipton, C., Scerri, E.M.L., Stimpson, C.M., Crassard, R., Hilbert, Y., Alsharekh, A., Al-Omari, A., Petraglia, M.D., 2015. Remote sensing and GIS techniques for reconstructing Arabian palaeohydrology and identifying archaeological sites. Quaternary International 382, 98-119.

Brown, G.F., 1960. Geomorphology of central and western Saudi Arabia. 21st International Geological Congress 150-159.

Brown, G.F., Schmidt, D.L., Huffman, Jr., A.C., 1989. Geology of the Arabian Peninsula – Shield Area of Western Saudi Arabia. U.S. Geological Survey Professional Paper 560A, 199pp.

Burns, S.J., Fleitmann, D., Matter, A., Neff, U., Mangini, A., 2001. Speleothem evidence from Oman for continental pluvial events during interglacial periods. Geology 29, 623-626.

Cailleux, A., 1952. Morphoskopische Analyse der Geschiebe und Sandkörner und ihre Bedeutung für die Paläoklimatologie. Geologische Rundschau 40, 11-19.

Camp, V.E., Roobol, M.J., 1989. The Arabian continental alkali basalt province: Part 1. Evolution of Harrat Rahat, Kingdom of Saudi Arabia. Bulletin of the Geological Society of America 101, 71-95.

Camp, V.E., Roobol, M.J., 1991. Geologic map of the Cenozoic lava field of Harrat Rahat, Kingdom of Saudi Arabia. Saudi Arabian Directorate of Mineral Resources Geosciences Map GM-123, scale 1 : 250,000, with text 37 pp.

Catlett, G.A., 2014. Pluvial deposits in Mudawwara, Jordan and their implications for Mediterranean and monsoonal precipitation in the Levant. M.Sc. Thesis, Miami University, Oxford, Ohio, 32 pp.

Clark, I.D., Fritz, P., 1967. Environmental Isotopes in Hydrogeology. New York, Boca Raton, Lewis Publishers, CRC Press LLC, 352 pp.

Crassard, R., Petraglia, M.D., Drake, N.A., Breeze, P., Gratuze, B., Alsharekh, A., Arbach, M., Groucutt, H.S., Khalidi, L., Michelsen, N., Robin, C.J., Schiettecatte, J., 2013. Middle Palaeolithic and Neolithic occupations around Mundafan palaeolake, Saudi Arabia: Implications for climate change and human dispersal. PLOS One 8, e69665.

Davies, C.P., 2006. Holocene paleoclimates of southern Arabia from lacustrine deposits of the Dhamar highlands, Yemen. Quaternary Research 66, 454-464.

Dinies, M., Plessen, B., Neef, R., Kürschner, H., 2015. When the desert was green: Grassland expansion during the early Holocene in northwestern Arabia. Quaternary International 382, 293-302.

Edgell, H.S., 1990. Evolution of the Rub' al Khali desert. Journal of King Abdulaziz University: Earth Sciences, vol. 3, Special Issue, 1st Saudi Symposium on Earth Sciences 1989, 81-93, Jeddah.

Edgell, H.S., 2006. Arabian Deserts. Nature, Origin and Evolution. Springer, Dordrecht, 592 pp.

Engel, M., Brückner, H., Pint, A., Wellbrock, K., Ginau, A., Voss, P., Grottker, M., Klasen, N., Frenzel, P., 2012. The early Holocene humid period in NW Saudi Arabia – Sediments, microfossils and palaeo-hydrological modelling. Quaternary International 266, 131-141.

Enzel, Y., Kushnir, Y., Quade, J., 2015. The middle Holocene climatic records from Arabia: Reassessing lacustrine environments, shift of ITCZ in Arabian Sea, and impacts of the southwest Indian and African monsoon. Global and Planetary Change 129, 69-91.

Farr, T.G., Kobrick, M., 2000. Shuttle radar topography mission produces a wealth of data. Eos, Transactions American Geophysical Union 81, 583.

Farr, T.G., Rosen, P.A., Caro, E., Crippen, R., Duren, R., Hensley, S., Kobrick, M., Paller, M., Rodriguez, E., Roth, L., Seal, D., Shaffer, S., Shimada, J., Umland, J., Werner, M., Oskin, M., Burbank, D., Alsdorf, D., 2007. The Shuttle Radar Topography Mission. Reviews of Geophysics 45, RG2004.

Fleitmann, D., Burns, S.J., Neff, U., Mangini, A., Matter, A., 2003a. Changing moisture sources over the last 330,000 years in Northern Oman from fluid-inclusion evidence in speleothems. Quaternary Research 60, 223-232.

Fleitmann, D., Burns, S.J., Mudelsee, M., Neff, U., Kramers, J., Mangini, A., Matter, A., 2003b. Holocene forcing of the Indian monsoon recorded in a stalagmite from Southern Oman. Science 300, 1737-1739.

Fleitmann, D., Matter, A., Pint, J., Al-Shanti, M.A., 2004. The speleothem record of climate change in Saudi Arabia. Open-File Report, SGS-OF-2004-8. Saudi Geological Survey. 40 pp.

Fleitmann, D., Burns, S.J., Neff, U., Mudelsee, M., Mangini, A., Kramers, J., Matter, A., 2005. Holocene records of rainfall variation and associated ITCZ migration from stalagmites from northern and southern Oman. In: Diaz, H.F., Bradley, R.S. (eds.), The Hadley Cell Circulation: Present, past and future, 259-287. Kluwer Academic Publishers. Dordrecht, The Netherlands.

Fleitmann, D., Burns, S.J., Mangini, A., Mudelsee, M., Kramers, J., Villa, I., Neff, U., Al-Subbary, A.A., Buettner, A., Hippler, D., Matter, A., 2007. Holocene ITCZ and Indian monsoon dynamics recorded in stalagmites from Oman and Yemen (Socotra). Quaternary Science Reviews 26, 170-188.

Fleitmann, D., Burns, S.J., Pekala, M., Mangini, A., Al-Subbary, A., Al-Aowah, M., Kramers, J., Matter, A., 2011. Holocene and Pleistocene pluvial periods in Yemen, southern Arabia. Quaternary Science Reviews 30, 783-787.

Frenzel, P., Schulze, I., Pint, A., 2012. Noding of *Cyprideis torosa* valves (Ostracoda) – a proxy for salinity? New data from field observations and a long-term microcosm experiment. International Review of Hydrobiology 97, 314-329.

Galbraith, R.F., Roberts, R.G., Laslett, G.M., Yoshida, H., Olley, J.M., 1999. Optical dating of single and multiple grains of quartz from Jinmium rock shelter, northern Australia, part 1, Experimental design and statistical models. Archaeometry 41, 339-364.

Ginau, A., Engel, M., Brückner, H., 2012. Holocene chemical precipitates in the continental sabkha of Tayma (NW Saudi Arabia). Journal of Arid Environments 84, 26-37.

Goward, S.N., Masek, J.G., Williams, D.L., Irons, J.R., Thompson, R.J., 2001. The Landsat 7 mission. Remote Sensing of Environment 78, 3–12.

Goudie, A.S., Colls, A., Stokes, S., Parker, A., White, K., Al-Farraj, A., 2000. Latest Pleistocene and Holocene dune construction at the north-eastern edge of the Rub' al Khali, United Arab Emirates. Sedimentology 47, 1011-1021.

Groucutt, H.S., White, T.S., Clark-Balzan, L., Parton, A., Crassard, R., Shipton, C., Jennings, R.P., Parkar, A.G., Breeze, P.S., Scerri, E.M.L., Alsharekh, A., Petraglia, M.D., 2015. Human occupation of the Arabian Empty Quarter during MIS 5: evidence from Mundafan Al-Bahayrah, Saudi Arabia. Quaternary Science Reviews 119, 116-135.

Guérin, G., Mercier, N., Adamiec, G., 2011. Dose-rate conversion factors: update. Ancient TL 29, 5-8.

Herold, M., Lohmann, G., 2009. Eemian tropical and subtropical African moisture transport: an isotope modelling study. Climate Dynamics 33, 1075-1088.

Hilbert, Y.H., White, T., Parton, A., Clark-Balzan, L., Crassard, R., Groucutt, H.S., Jennings, R.P., Breeze, P., Parker, A., Shipton, C., Al-Omari, A., Alsharekh, A., Petraglia, M.D., 2014. Epipalaeolithic occupation and palaeoenvironments of the southern Nefud desert, Saudi Arabia, during terminal Pleistocene and Early Holocene. Journal of Archaeological Science 50, 460-474.

Hoffmann, G., Rupprechter, M., Rahn, M., Preusser, F., 2015. Fluvio-lacustrine deposits reveal precipitation pattern in SE Arabia during early MIS 3. Quaternary International 382, 145-153.

Holm, D.A., 1960. Desert geomorphology in the Arabian Peninsula. Science 132, 1369-1379.

Hötzl, H., Maurin, V., Zötl, J.G., 1978a. Geologic history of the Al Hasa area since the Pliocene. In: Al-Sayari, S.S., Zötl, J.G. (eds.): Quaternary Period in Saudi Arabia, 58-77. Wien, Springer-Verlag.

Hötzl, H., Felber, H., Maurin, V., Zötl, J.G., 1978b. Accumulation terraces of Wadi Hanifa and Wadi Al Luhy. In: Al-Sayari, S.S., Zötl, J.G. (eds.): Quaternary Period in Saudi Arabia, 202-209. Wien, Springer-Verlag.

Huntley, D.J., Baril, M.R., 1997. The K content of the K-feldspars being measured in optical dating or in thermoluminescence dating. Ancient TL 15, 11-14.

Jennings, R.P., Singarayer, J., Stone, E.J., Krebs-Kanzow, U., Khon, V., Nisancioglu, K.H., Pfeiffer, M., Zhang, X., Parker, A., Parton, A., Groucutt, H.S., White, T.S., Drake, N.A., Petraglia, M.D., 2015. The greening of Arabia: Multiple opportunities for human occupation of the Arabian Peninsula during the Late Pleistocene inferred from an ensemble of climate model simulations. Quaternary International 382, 181-199.

Jenson, S. K., Domingue, J. O., 1988. Extracting topographic structure from digital elevation data for Geographic Information System Analysis. Photogrammetric Engineering and Remote Sensing 54, 1593–1600.

Juyal, N., Singhvi, A.K., Glennie, K.W., 1998. Chronology and palaeoenvironmental significance of Quaternary desert sediment in southeastern Arabia. In: Alsharan, A.S., Glennie, K.W., Whittle, G.L., Kendall, C.G.St.C. (eds.), Quaternary Deserts and Climate Change, 315-325, Rotterdam, Balkema.

Krinsley, D.H., Doornkamp, J.C., 1973. Atlas of quartz sand surface textures. Cambridge, University Press, 91pp.

Lézine, A.-M., Saliège, J.-F., Robert, C., Wertz, F., Inizan, M.-L., 1998. Holocene lakes from Ramlat as-Sab'atayn (Yemen) illustrate the impact of monsoon activity in southern Arabia. Quaternary Research 50, 290-299.

Lézine, A.-M., Robert, C., Cleuziou, S., Inizan, M.-L., Braemer, F., Saliège, J.-F., Sylvestre, F., Tiercelin, J.-J., Crassard, R., Méry, S., Carpentier, V., Steimer-Herbst, T., 2010. Climate change and human occupation in the Southern Arabian lowlands during the last deglaciation and the Holocene. Global and Planetary Change 72, 412-428.

Lopes-Lima, M., Seddon, M.B., 2014. *Unio tigridis*. The IUCN red list of threatened species, version 2015.2. www.iucnredlist.org. Downloaded on 28 August 2015.

Lowick, S.E., Trauerstein, M., Preusser, F. 2012. Testing the application of post IR-IRSL dating to fine grain waterlain sediments. Quaternary Geochronology 8, 33-40.

Matter, A., Neubert, E., Preusser, F., Rosenberg, T.M., Al-Wagdani, K., 2015. Palaeo-environmental implications derived from lake and sabkha deposits of the southern Rub' al-Khali, Saudi Arabia and Oman. Quaternary International 382, 120-131.

McClure, H.A., 1976. Radiocarbon chronology of Late Quaternary lakes in the Arabian desert. Nature 263, 755-756.

McClure H. A., 1984. Late Quaternary palaeoenvironments of the Rub’al Khali. PhD thesis, London, University of Central London (unpublished), 245pp.

McClure, H.A., Swain, F.M., 1980. Fresh-water and brackish-water fossil Quaternary Ostracoda from the Rub’ al Khali (“Empty Quarter”), Saudi Arabia. Actes du VI^{e} Colloque Africain de Micropaléontologie, Tunis, 1974. Annales des Mines et de la Géologie, Tunis, 28, tome III, 427-441.

McLaren, S.J., Al-Juaidi, F., Bateman, M.D., Millington, A.C., 2009. First evidence for episodic flooding in the arid interior of central Saudi Arabia over the last 60 ka. Journal of Quaternary Science 24, 198-207.

Meisch, C., 2000. Freshwater ostracoda of western and central Europe. Süsswasserfauna von Mitteleuropa, vol. 8 Crustacea. Schwoerbel, J., Zwick, P. (eds.). Spektrum Akademischer Verlag, 522pp.

Murray, A.S., Wintle, A.G., 2000. Luminescence dating of quartz using an improved single-aliquot regenerative-dose protocol. Radiation Measurements 32, 57-73.

Neff, U., Burns, S.J., Mangini, A., Mudelsee, M., Fleitmann, D., Matter, A., 2001. Strong coherence between solar variability and the monsoon between 9 and 6 kyr ago. Nature 411, 290-293.

Neubert, E., 1998. Annotated checklist of the terrestrial and freshwater Molluscs of the Arabian Peninsula. Fauna of Arabia, 17, 333–461. Basel/Riyadh.

Neubert, E., Amr, Z., van Damme, D., 2015. Chapter 4: The status and distribution of freshwater molluscs in the Arabian Peninsula. In: Garcìa, N., Harrison, I., Cox, N., Tognelli, M.F. (compilers): The status and distribution of the freshwater biodiversity in the Arabian Peninsula: 30-38, Appendix 2. Gland, Switzerland, Cambridge, UK., Arlington, USA:IUCN.

Parker, A.G., Eckersley, L., Smith, M.M., Goudie, A.S., Stokes, S., Ward, S., White, K., Hodson, M.J., 2004. Holocene vegetation dynamics in the north-eastern Rub’ al-Khali desert, Arabian Peninsula: a phytolith, pollen and carbon isotope study. Journal of Quaternary Science 19, 665-676.

Parker, A.G., Goudie, A.S., Stokes, S., White, K., Hodson, M.J., Manning, M., Kennet, D., 2006. A record of Holocene climate change from lake geochemical analyses in southeastern Arabia. Quaternary Research 66, 465-476.

Parton, A., Farrant, A.R., Leng, M.J., Telfer, M.W., Groucutt, H.S., Petraglia, M.D., Parker, A., 2015. Alluvial fan records from southeast Arabia reveal multiple windows for human dispersal. Geology 43, 295-298.

Petit-Maire, N., Carbonel, P., Reyss, J.L., Sanlaville, P., Abed, A., Bourrouilh, R., Fontugne, M., Yasin, S., 2010. A vast palaeolake in Southern Jordan (29 N). Global and Planetary Change 72, 368-373.

Petraglia, M.D., Alsharekh, A.M., Crassard, R., Drake, N.A., Groucutt, H., Parker, A.G., Roberts, R.G., 2011. Middle Palaeolithic occupation on a Marine Isotope Stage 5 lakeshore in the Nefud Desert, Saudi Arabia. Quaternary Science Reviews 30, 1555-1559.

Petraglia, M.D., Alsharekh, A., Breeze, P., Clarkson, C., Crassard, R., Drake, N.A., Groucutt, H.S., Jennings, R., Parker, A.G., Parton, A., Roberts, R.G., Shipton, C., Matheson, C., Al-Omari, A., Veal, M.-A., 2012. Hominin dispersal into the Nefud desert and middle Palaeolithic settlement along the Jubbah palaeolake, northern Arabia. PLoS ONE 7, e49840, doi: 10.371/journal.ponr,0049840.

Philby, H.St.J.B., 1933. The Empty Quarter. Constable & Company Ltd, London, 433pp.

Philippsen, B., 2013. The freshwater reservoir effect in radiocarbon dating. Heritage Science 1, 24pp.

Pint, A., Frenzel, P., Fuhrmann, R. Scharf, B., Wennrich, V., 2012. Distribution of *Cyprideis torosa* (Ostracoda) in Quaternary athalassic sediments in Germany and its application for palaeoecological reconstructions. International Review of Hydrobiology 97, 330-355.

Prescott, J., Hutton, J.T., 1994. Cosmic ray contributions to dose rates for luminescence and ESR dating: Large depths and long-term time variations. Radiation Measurements 23, 497-500.

Preusser, F., Kasper, H.U., 2001. Comparison of dose rate determination using high-resolution gamma spectrometry and inductively coupled plasma-mass spectrometry. Ancient TL 19, 19-24.

Preusser, F., Radies, D., Matter, A., 2002. A 160,000-year record of dune development and atmospheric circulation in southern Arabia. Science 296, 2018-2020.

Preusser, F., Chithambo, M.L., Götte, T., Martini, M., Ramseyer, K., Sendezera, E.J., Susino, G.J., Wintle, A.G., 2009. Quartz as a natural luminescence dosimeter. Earth Science Reviews 97, 196–226.

Preusser, F., Muru, M., Rosentau, A., 2014. Comparing different post-IR IRSL approaches for the dating of Holocene foredunes from Ruhnu Island, Estonia. Geochronometria 41, 342-351.

Rabus, B., Eineder, M., Roth, A., Bamler, R., 2003. The shuttle radar topography mission-a new class of digital elevation models acquired by spaceborne radar. Journal of Photogrammetry & Remote Sensing 57, 241-262.

Radies, D., Preusser, F., Matter, A., Mange, M., 2004. Eustatic and climatic controls on the development of the Wahiba sand sea, Sultanate of Oman. Sedimentology 51, 1359-1385.

Radies, D., Hasiotis, S.T., Preusser, F., Neubert, E., Matter, A., 2005. Paleoclimatic significance of Early Holocene faunal assemblages in wet interdune deposits of the Wahiba sand sea, Sultanate of Oman. Journal of Arid Environments 62, 109-125.

Reimann, T., Tsukamoto, S., 2012. Dating the recent past (<500 years) by post-IR IRSL feldspar - Examples from the North Sea and Baltic Sea coast. Quaternary Geochronology 10, 180-187.

Reimer, P. J., Bard, E., Bayliss, A., Beck, J. W., Blackwell, P. G., Bronk Ramsey, C., Buck, C. E., Cheng, H., Edwards, R. L., Friedrich, M., Grootes, P. M., Guilderson, T. G., Haflidason, H., Hajdas, I., Hatté, C., Heaton, T. J., Hoffmann, D. L., Hogg, A. G., Hughen, K. A., Kaiser, K. F., Kromer, B., Manning, S. W., Niu, M., Reimer, R. W., Richards, D. A., Scott, E. M., Southon, J. R., Staff, R. A., Turney, C. S. M., van der Plicht, J., 2013. IntCal13 and Marine13 radiocarbon age calibration curves 0–50,000 years cal References BP. Radiocarbon 55, 1869-1887.

Richter, D., Richter, A., Dornich, K., 2013. Lexsyg - A new system for luminescence research. Geochronometria 40, 220-228.

Rosenberg, T.M., Preusser, F., Blechschmidt, I., Fleitmann, D., Jagher, R., Matter, A., 2011a. Late Pleistocene palaeolake in the interior of Oman: a potential key area for the dispersal of anatomically modern humans out-of-Africa? Journal of Quaternary Science 27, 13-16.

Rosenberg, T.M., Preusser, F., Fleitmann, D., Schwalb, A., Penkman, K., Schmid, T.W., Al-Shanti, M.A., Kadi, K., Matter, A., 2011b. Late Pleistocene pluvial periods in southern Arabia: windows of opportunity for modern human dispersal. Geology 39, 1115-1118.

Rosenberg, T.M., Preusser, F., Risberg, J., Plikk, A., Kadi, K.A., Matter, A., Fleitmann, D., 2013. Middle and late Pleistocene humid periods recorded in palaeolake deposits of the Nafud desert, Saudi Arabia. Quaternary Science Reviews 70, 109-123.

Scerri, E.M.L., Breeze, P., Parton, A., Groucutt, H.S., White, T.S., Stimpson, C., Clark-Balzan, L., Jennings, R., Alsharekh, A., Petraglia, M.D., 2015. Middle to late Pleistocene human habitation in the western Nefud desert, Saudi Arabia. Quaternary International 382, 200-214.

Schulz, E., Whitney, J.W., 1986. Upper Pleistocene and Holocene lakes in the An Nafud, Saudi Arabia. Hydrobiologia 143, 175-190.

Stimpson, C., Breeze, P., Clark-Balzan, L., Groucutt, H.S., Jennings, R., Parton, A., Scerri, E., White, T.S., Petraglia, M.D., 2015. Stratified Pleistocene vertebrates with a new record of jaguar-sized pantherine (*Panthera cf. gombaszogensis*) from northern Saudi Arabia. Quaternary International 382, 168-180.

Szidat, S., Salazar, G. A., Vogel, E., Battaglia, M., Wacker, L., Synal, H.-A., Türler, A., 2014. ^{14}C analysis and sample preparation at the new Bern Laboratory for the Analysis of Radiocarbon with AMS (LARA). Radiocarbon 56, 561-566.

Tachikawa, T., Kaku, M., Iwasaki, A., Gesch, D., Oimoen, D., Zhang, Z., Danielson, J., Krieger, T., Curtis, B., Haase, J., Abrams, M., Crippen, R., and Carabajal, C., 2011. ASTER Global Digital Elevation Model Version 2 – Summary of Validation Results. METI & NASA, 26pp.

Vincent, P., 2008. Saudi Arabia: An Environmental Overview. London, Taylor & Francis Group, 309pp.

Wacker, L., Fülöp, R.-H., Hajdas I., Molnár, M., Rethemeyer, J., 2013. A novel approach to process carbonate samples for radiocarbon measurements with helium carrier gas. Nucl. Instrum. Methods B 294, 214-217.

Wallinga, J., Bos, A.J.J., Dorenbos, P., Murray, A.S., Schokker, J., 2007. A test case for anomalous fading correction in IRSL dating. Quaternary Geochronology 2, 216–221.

Webster, P.J., 2005. The elementary Hadley circulation. In: Diaz, H.F., Bradley, R.S. (eds.), The Hadley Cell Circulation: Present, Past and Future, 9-60. Kluwer Academic Publishers, Dordrecht, The Netherlands.

Whitney, J.W., 1983. Erosional history and surficial geology of Western Saudi Arabia. Technical Record, USGS-TR-03-1, 90pp.

Wilson, I. G., 1973. Ergs. Sedimentary Geology 10, 77-106.

Wintle, A.G., Murray, A.S., 2006. A review of quartz optically stimulated luminescence characteristics and their relevance in single-aliquot regeneration dating protocols. Radiation Measurements 41, 369-391.

Zander, A., Degering, D., Preusser, F., Kasper, H.U., Brückner, H., 2007. Optically stimulated luminescence dating of sublittoral and intertidal sediments from Dubai, UAE.: Radioactive disequilibria in the uranium decay series. Quaternary Geochronology 2, 123-128.

Table 1. Radiocarbon dating results. Uncalibrated ^{14}C ages are given with one sigma uncertainty. They are calibrated using the IntCal13 dataset (Reimer et al., 2013) and presented as age ranges representing 2σ confidence limits. * Significant calcite contribution indicates post-depositional precipitation of carbonates, age is considered as minimum estimate.

Sample	Material	Lab Code	Uncalibrated ^{14}C age (yr BP)	Calendar age range (2σ) (yr BP)
4213.1	*Unio tigridis*	BE-2751	6630 ± 50	7430-7590
4213.1	*Melanoides tuberculata*	BE-2752	6600 ± 60	7420-7580
4213.2	*Unio tigridis*	BE-2753	7740 ± 60	8410-8610
4213.2	*Melanoides tuberculata*	BE-2754	7640 ± 70	8350-8580
4213.3	*Unio tigridis*	BE-2755	6360 ± 50	7170-7420
4213.3	*Melanoides tuberculata*	BE-2756	7430 ± 70*	(8050-8380)
4214.2	*Bulinus*	BE-2757	7930 ± 60	8610-8990
4214.3	*Unio tigridis*	BE-2758	7770 ± 60	8410-8650
4214.3	*Melanoides tuberculata*	BE-2759	7760 ± 70	8400-8700

Table 2. Summary data of luminescence dating with sampling depth below surface, the grain size used for Equivalent dose (D_e) determination, the number of aliquots used for calculation of mean D_e, and the concentration of dose rate relevant elements (K, Th, U). U-238 = concentration of Uranium as deduced from the U-235 peak at 186 keV, U-post Ra = as deduced from post-Ra-226 isotopes Bi-214 and Pb-214 (cf. Preusser and Kasper, 2001; Zander et al., 2007). Given is the total annual dose rate (D) for both IRSL/pIR and OSL, observed overdispersion, the age model (C = Central Age Model, M = Minimum Age Model) being used and the resulting mean D_e and age for the three different approaches.

Sample	Depth (cm)	Grain size (µm)	n F/Q	K (%)	Th (ppm)	U-238 (ppm)	U-post Ra (ppm)	D IRSL (Gy ka^{-1})	D OSL (Gy ka^{-1})	od (%)	Model	D_e IRSL (Gy)	D_e pIR (Gy)	D_e OSL (Gy)	Age IRSL (ka)	Age pIR (ka)	Age OSL (ka)
4213.1/1	36	200-250	13/19	0.59 ± 0.01	1.12 ± 0.05	0.15 ± 0.08	0.38 ± 0.01	1.71 ± 0.12	0.90 ± 0.04	0.16/0.27/0.22	C/M/M	6.88 ± 0.32	9.25 ± 0.27	5.49 ± 0.25	4.0 ± 0.3	5.4 ± 0.4	6.1 ± 0.4
4213.2/1	50	200-250	12/22	0.94 ± 0.01	1.42 ± 0.07	0.48 ± 0.19	0.49 ± 0.03	2.07 ± 0.11	1.26 ± 0.05	0.23/0.42/0.18	M/M/M	12.20 ± 0.72	16.38 ± 0.91	9.31 ± 0.29	5.9 ± 0.5	7.9 ± 0.6	7.4 ± 0.4
4213.3/1	56	200-250	10/21	0.77 ± 0.01	0.95 ± 0.03	0.57 ± 0.24	0.33 ± 0.01	1.87 ± 0.09	1.05 ± 0.05	0.22/0.42/0.45	C/M/M	9.53 ± 0.67	11.98 ± 0.73	6.17 ± 0.30	5.1 ± 0.5	6.4 ± 0.5	5.9 ± 0.4
4213.3/2	30	200-250	13/22	1.07 ± 0.02	3.91 ± 0.12	0.60 ± 0.70	1.35 ± 0.04	2.61 ± 0.09	1.78 ± 0.13	0.18/0.26/0.20	M/M/M	8.20 ± 0.24	10.43 ± 0.38	6.60 ± 0.23	3.1 ± 0.2	4.0 ± 0.2	3.7 ± 0.3
4214.1/1	36	200-250	12/27	1.11 ± 0.02	1.20 ± 0.05	0.30 ± 0.20	0.55 ± 0.02	2.26 ± 0.14	1.46 ± 0.05	0.43/0.18/0.41	C/C/C	175.1 ± 22.0	245.9 ± 19.7	81.71 ± 6.82	77 ± 11	109 ± 11	>56 ± 5
4214.2/1	50	200-250	12/25	1.19 ± 0.02	1.86 ± 0.06	0.77 ± 0.14	0.59 ± 0.01	2.38 ± 0.10	1.57 ± 0.05	0.38/0.10/0.35	C/C/C	133.9 ± 23.0	214.0 ± 10.8	98.97 ± 7.20	56 ± 10	90 ± 6	>63 ± 5
4214.3/1	200	200-250	12/22	1.08 ± 0.01	3.82 ± 0.11	1.47 ± 0.17	1.11 ± 0.04	2.40 ± 0.13	1.68 ± 0.06	0.12/0.04/0.13	C/C/C	11.31 ± 0.43	14.01 ± 0.23	10.25 ± 0.34	4.5 ± 0.3	5.6 ± 0.3	6.1 ± 0.3
4216.1/1	140	200-250	13/10	1.60 ± 0.02	2.35 ± 0.12	0.87 ± 0.21	0.77± 0.02	2.06 ± 0.12	-	0.33/0.56/-	M/M/-	12.93 ± 0.67	14.64 ± 1.16	med. comp.	6.3 ± 0.4	7.1 ± 0.7	-
4216.2/1	150	200-250	11/10	1.67 ± 0.02	1.53 ± 0.02	0.48 ± 0.11	0.50 ± 0.02	2.77 ± 0.10	-	0.10/0.16/-	C/M/-	61.35 ± 2.08	82.66 ± 3.32	med. comp.	22.2 ± 1.1	29.8 ± 1.6	-

Figures

Fig. 1. a) Digital elevation model of the Arabian Peninsula derived from SRTM data. b) Palaeodrainage network and catchment areas of Wadi ad Dawasir and Wadi as Sahba systems, including the locations of sites and Figs. 2 and 3 (superimposed over SRTM elevation data, DEM on shaded-relief map). The DEM-derived drainage network (contributing area of >150 km²) was combined and complemented by other river courses than were inferred from the flow directions in areas with intermittent dune coverage (see examples in Fig. 2). Large sink areas and dune-dominated areas with interdune depressions deliver erroneous stream lines within the derived drainage network and were removed.

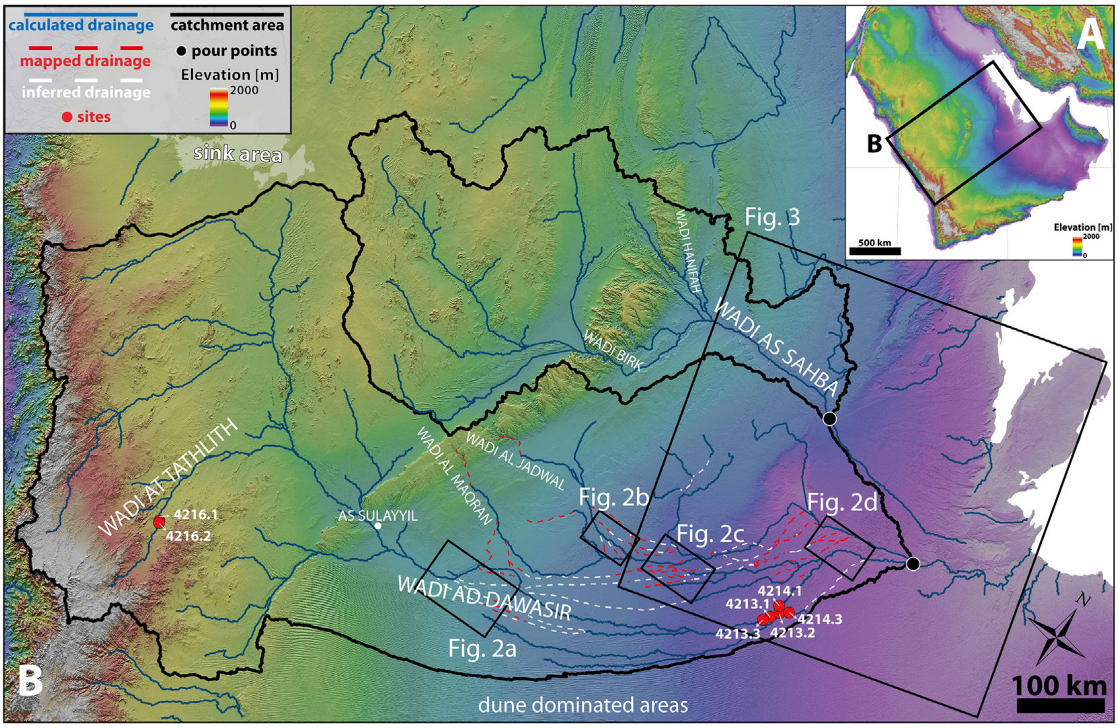

Fig. 2. Example areas with only minor or incomplete sand coverage. Landsat 7 FCCs clearly show a stark contrast between sand coverage and underlying palaeodrainage systems that were used to determine (A) and map (C) recent and palaeostream systems as well as flow directions (B) (RGB composites with a band combination of 7/4/2 and 3/2/1, histograms are stretched to display extent). Digital elevation data and derived hillshade images were additionally used to retrace drainage systems if underlying palaeochannels lead to inverse topography (D) (SRTM DEM on shaded-relief map).

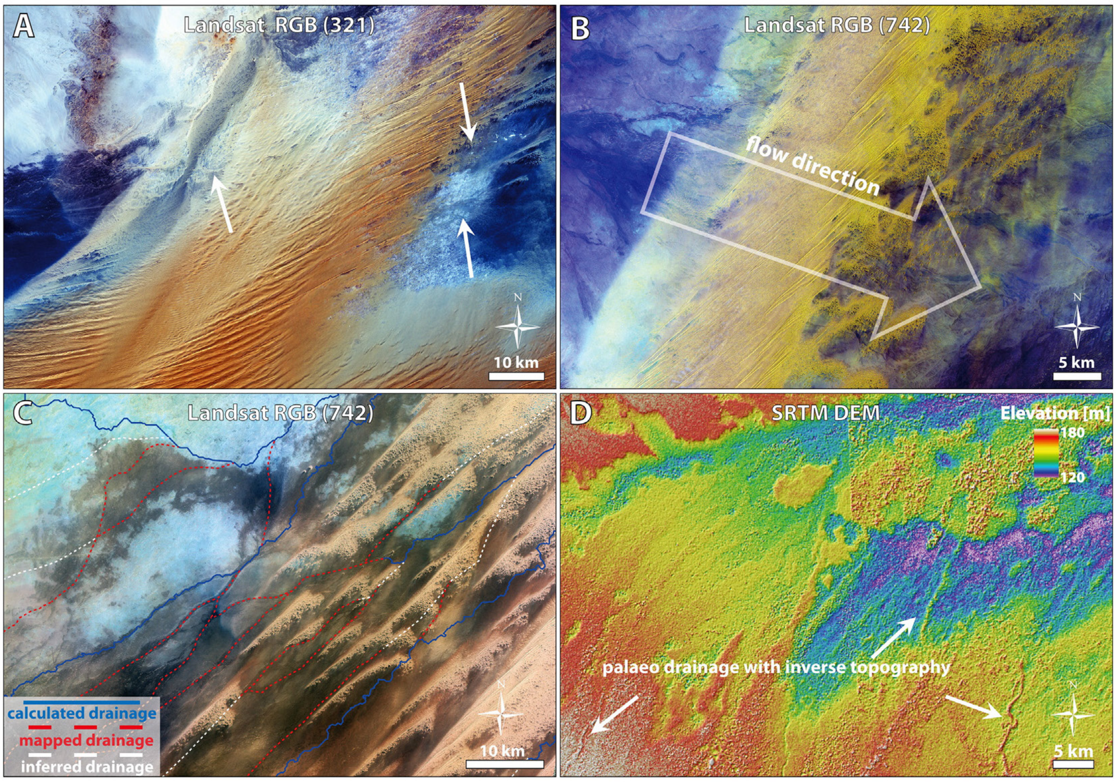

Fig. 3. Map of drainage network and catchment areas of downstream areas of Wadi ad Dawasir and Wadi as Sahba systems (superposed over SRTM elevation data, DEM on shaded-relief map). The Sahba fan acts as barrier forcing the Dawasir channels to flow eastwards into the western margin of the Sabkha Matti. The present day channel of Wadi as Sahba runs across the fan towards the Al Humr lake, but the large extent of the Sahba fan indicate a high erosion rate, high runoff and transport capacity in former times.

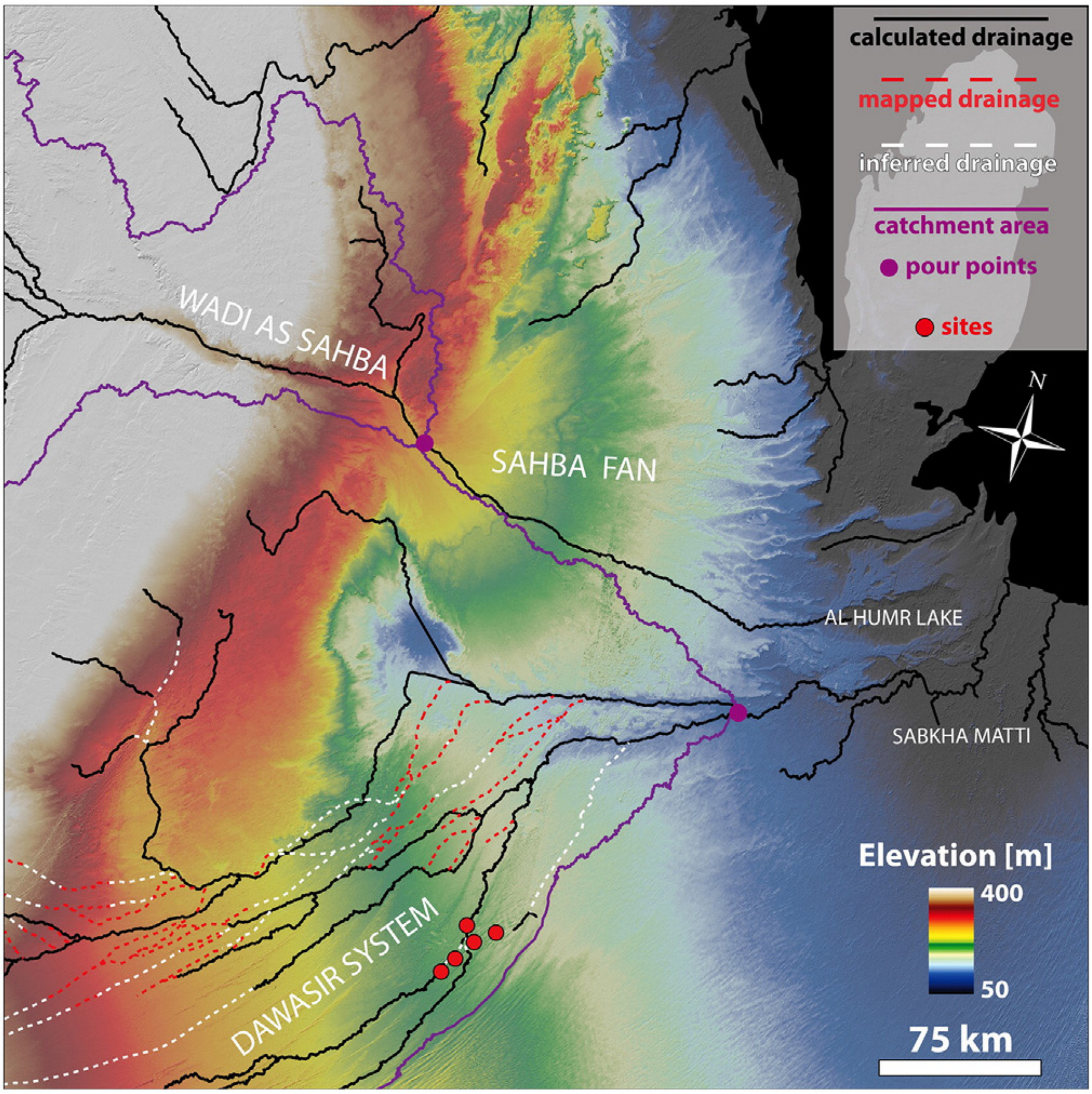

Fig. 4. Characterisation of the luminescence properties of the investigated samples: a) OSL decay curve of sample 13.2/1 exemplifying the dominance of the fast component in most of the samples; b) OSL decay curve of sample 16.1/1 revealing low signal level and the strong presence of a medium component; c) typical IRSL and d) typical pIR decay curves shown for sample 4214.2/1; e) OSL dose response curve close to saturation and f) pIR dose response of the sample 4214.2/1.

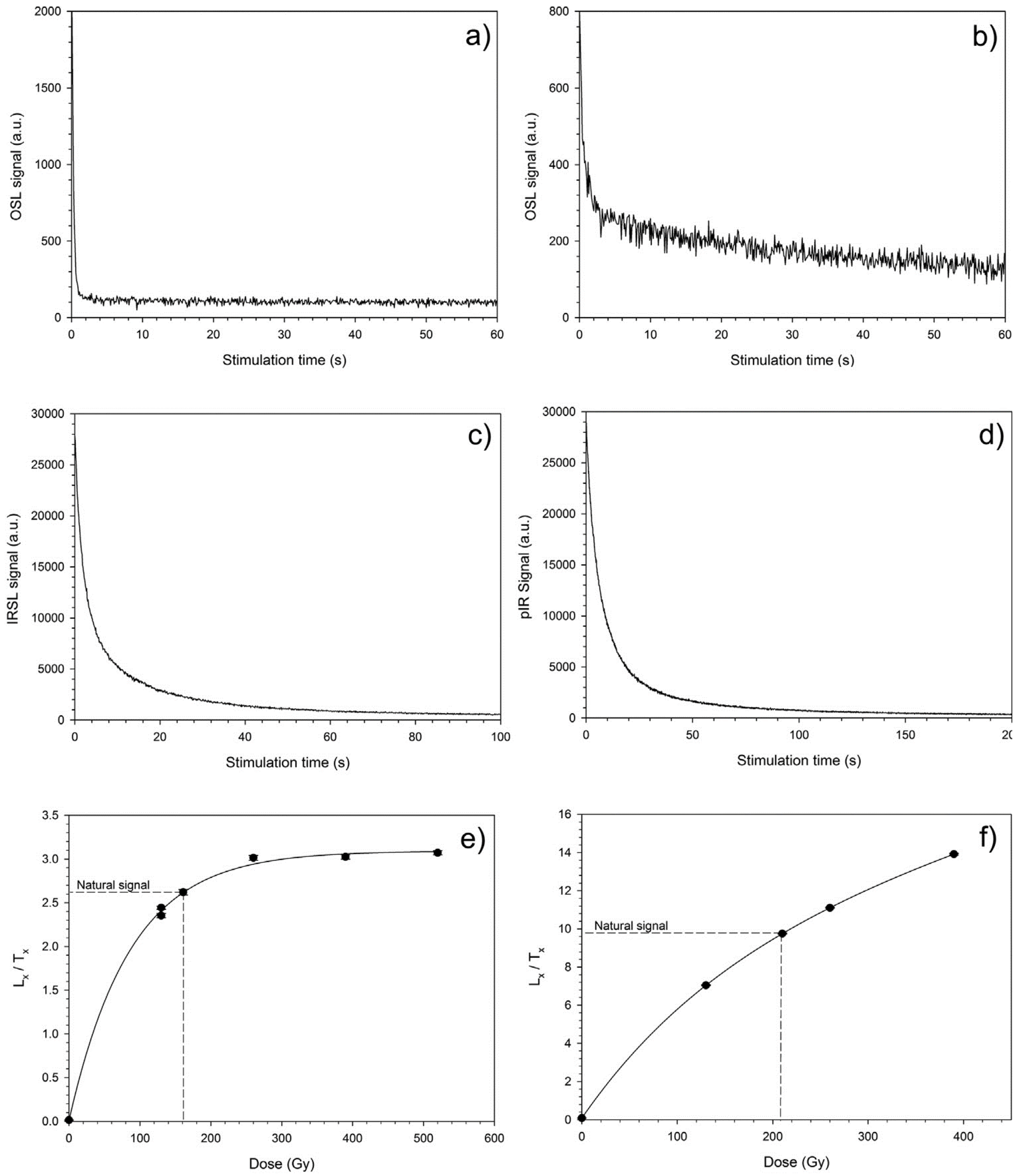

Fig. 5. Two examples of OSL D_e distributions for samples a) 4213.1/1 and b) 4213.3/3.

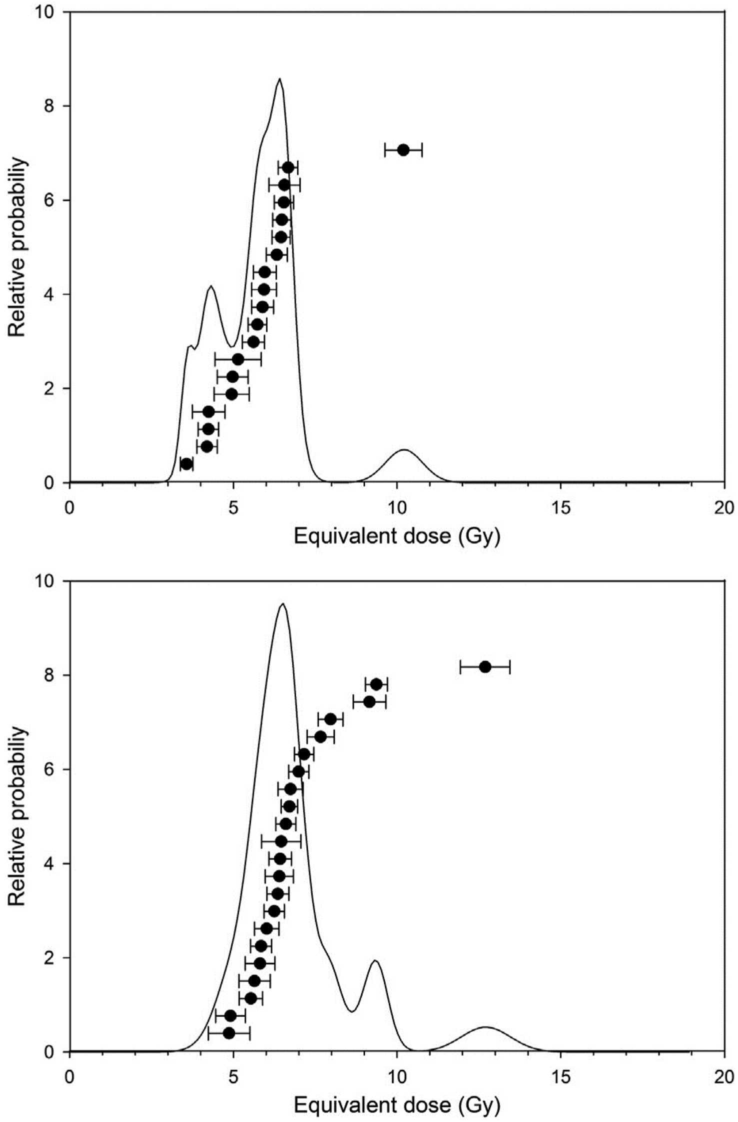

Fig. 6. Vertical lithological sections in the distal Wadi ad Dawasir. For locations see Fig. 1B and for legend Fig. 8. Grain size classification abbreviations: crsSU Coarse Sand (Upper) 710-1000 µm; crsSL Coarse Sand (Lower) 500-710 µm; mSU Medium Sand (Upper) 350-500 µm; mSL Medium Sand (Lower) 250-350 µm; fSU Fine Sand (Upper) 177-25 µm.

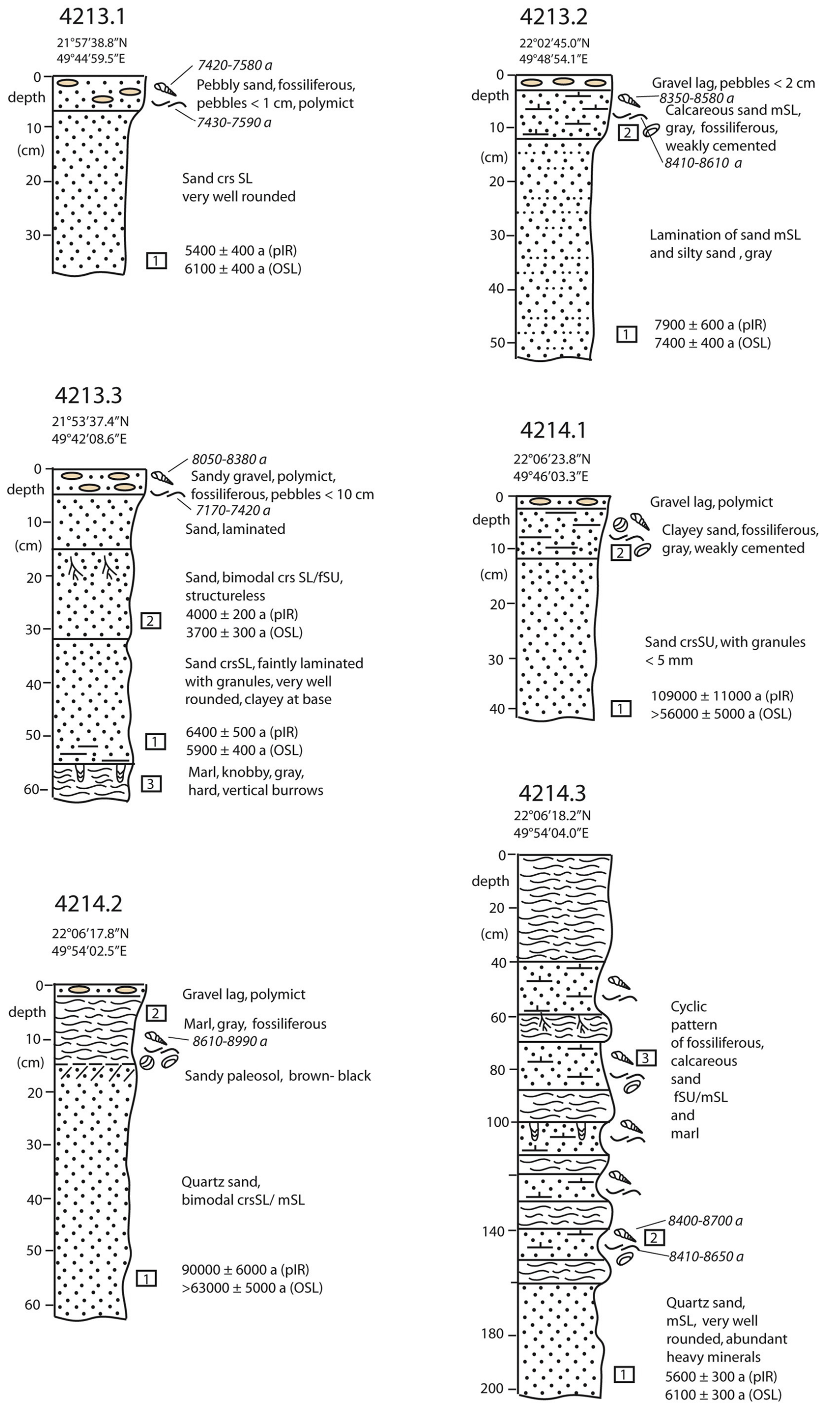

Fig. 7. Bing map satellite view showing location of site 4213.3 in Holocene channel partly covered by younger linear dune (A), photographs showing surface with pebble lag, *M. tuberculata* and *U. tigridis* in-situ position measuring 4 cm (B) of relict channel at site 4213.2 (C). Outcrop view of relict lacustrine section site 4214.3 measuring 2 metres (D). Photograph of vertical fluvial section in lower terrace at site 4216.1 in Wadi at Tathlith with pedogenic horizons. Note hammer for scale (E). Panoramic view looking E across ponded Holocene alluvial sandy silts in Wadi at Tathlith, 30 km upstream of site 4216.1 (F).

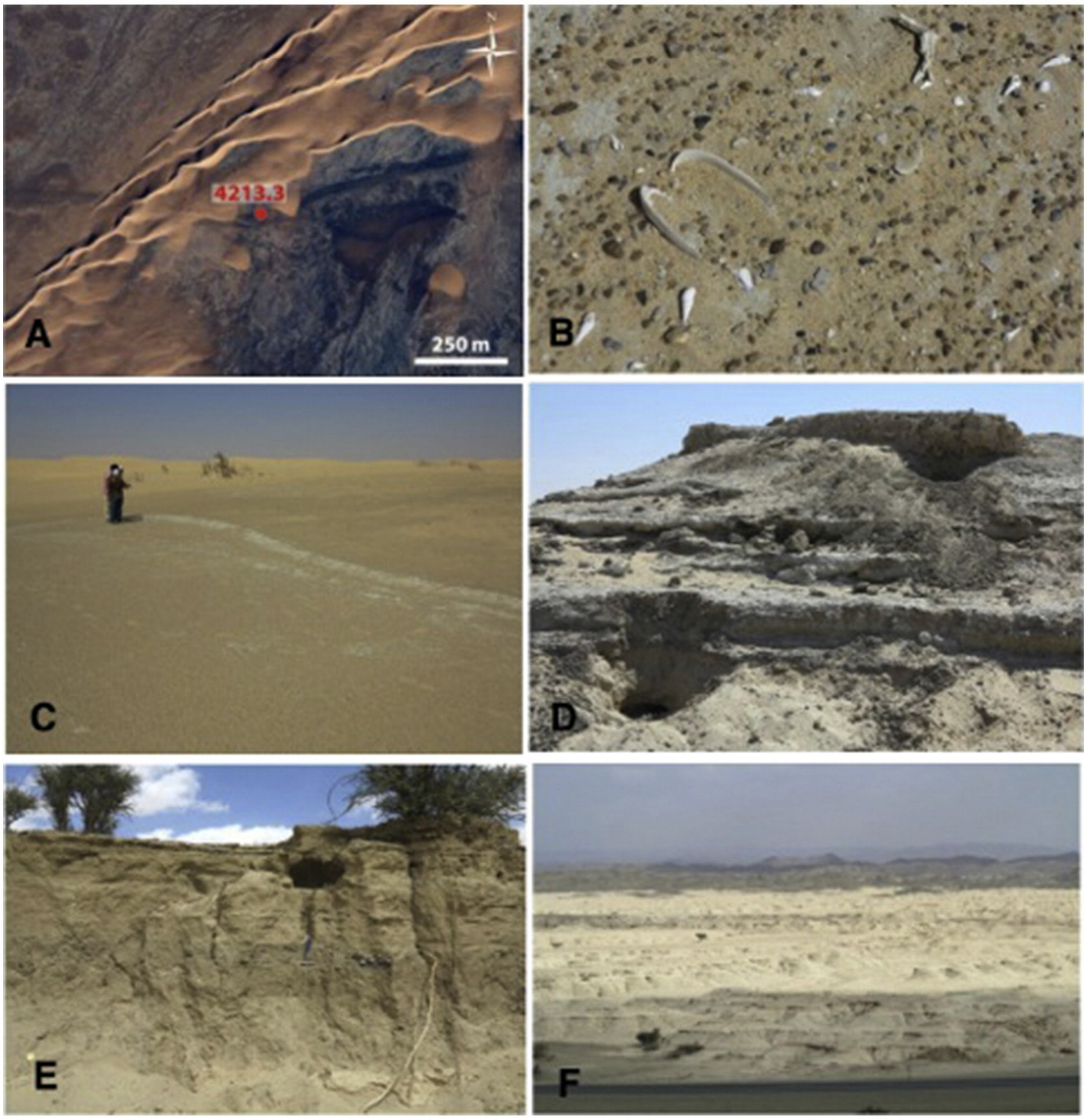

Fig. 8. Vertical lithological sections in Wadi at Tathlith. For locations see Fig. 1B.

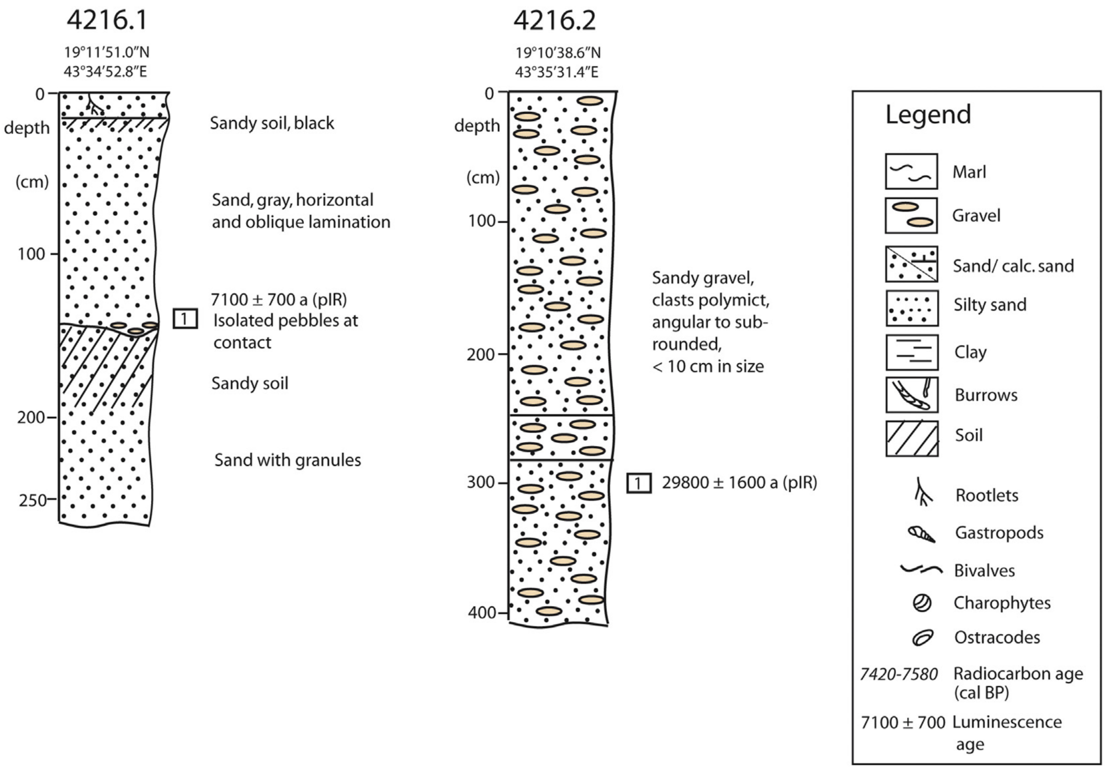

Fig. 9. OSL and pIR ages plotted in comparison to radiocarbon ages and revealing the substantial off-set between the methods. A significant calcite contribution indicates post-depositional precipitation of carbonates for sample 4213.3 *Melanoides tuberculata*. The curve on top is the isotope signature of a stalagmite from Qunf cave (Fleitmann et al., 2007), showing the gradual decrease in precipitation in southern Arabia during the middle Holocene.